

NASA TECHNICAL NOTE

NASA TN D-8329



NASA TN D-8329 *cl*

IN COPY: REI
AFWL TECHNICAL
KIRTLAND AFB,



RECERTIFICATION OF THE AIR AND METHANE STORAGE VESSELS AT THE LANGLEY 8-FOOT HIGH-TEMPERATURE STRUCTURES TUNNEL

*C. Michael Hudson, Robert L. Girouard,
Clarence P. Young, Jr., Dennis H. Petley,
John L. Hudson, Jr., and James L. Hudgins*

*Langley Research Center
Hampton, Va. 23665*





0134024

1. Report No. NASA TN D-8329		2. Government Accession No.		3. Recipient's Catalog No.	
4. Title and Subtitle RECERTIFICATION OF THE AIR AND METHANE STORAGE VESSELS AT THE LANGLEY 8-FOOT HIGH-TEMPERATURE STRUCTURES TUNNEL		5. Report Date February 1977		6. Performing Organization Code	
		8. Performing Organization Report No. L-11015		10. Work Unit No. 023-10-01-01	
7. Author(s) C. Michael Hudson, Robert L. Girouard, Clarence P. Young, Jr., Dennis H. Petley, John L. Hudson, Jr., and James L. Hudgins		11. Contract or Grant No.		13. Type of Report and Period Covered Technical Note	
9. Performing Organization Name and Address NASA Langley Research Center Hampton, VA 23665		14. Sponsoring Agency Code		15. Supplementary Notes	
12. Sponsoring Agency Name and Address National Aeronautics and Space Administration Washington, DC 20546		16. Abstract The Langley Research Center of the National Aeronautics and Space Administration is a leading aerospace research center. This center operates a number of sophisticated wind tunnels in order to fulfill the needs of its researchers. Compressed air, which is kept in steel storage vessels, is used to power many of these tunnels. Some of these vessels have been in use for many years, and Langley is currently recertifying these vessels to insure their continued structural integrity. One of the first facilities to be recertified under this program was the Langley 8-foot high-temperature structures tunnel. This recertification involved (a) modification, hydrotesting, and inspection of the vessels; (b) repair of all relevant defects; (c) comparison of the original design of the vessel with the current-design criteria of Section VIII, Division 2, of the 1974 ASME Boiler and Pressure Vessel Code; (d) fracture-mechanics, thermal, and wind-induced vibration analyses of the vessels; and (e) development of operating envelopes and a future inspection plan for the vessels. Following these modifications, analyses, and tests, the vessels were recertified for operation at full design pressure (41.4 MPa (6000 psi)) within the operating envelope developed.			
17. Key Words (Suggested by Author(s)) Pressure-vessel recertification Fracture-mechanics analysis Thermal analysis Vibration analysis Nondestructive examination ASME Code comparisons		18. Distribution Statement Unclassified - Unlimited Subject Category 37			
19. Security Classif. (of this report) Unclassified	20. Security Classif. (of this page) Unclassified	21. No. of Pages 75	22. Price* \$4.25		

RECERTIFICATION OF THE AIR AND METHANE STORAGE VESSELS AT THE
LANGLEY 8-FOOT HIGH-TEMPERATURE STRUCTURES TUNNEL

C. Michael Hudson, Robert L. Girouard, Clarence P. Young, Jr.,
Dennis H. Petley, John L. Hudson, Jr., and James L. Hudgins
Langley Research Center

SUMMARY

The Langley Research Center of the National Aeronautics and Space Administration is a leading aerospace research center. This center operates a number of sophisticated wind tunnels in order to fulfill the needs of its researchers. Compressed air, which is kept in steel storage vessels, is used to power many of these tunnels. Some of these vessels have been in use for many years, and Langley is currently recertifying these vessels to insure their continued structural integrity. One of the first facilities to be recertified under this program was the Langley 8-foot high-temperature structures tunnel. This recertification involved (a) modification, hydrotesting, and inspection of the vessels; (b) repair of all relevant defects; (c) comparison of the original design of the vessel with the current-design criteria of Section VIII, Division 2, of the 1974 ASME Boiler and Pressure Vessel Code; (d) fracture-mechanics, thermal, and wind-induced vibration analyses of the vessels; and (e) development of operating envelopes and a future inspection plan for the vessels. Following these modifications, analyses, and tests, the vessels were recertified for operation at full design pressure (41.4 MPa (6000 psi)) within the operating envelope developed.

INTRODUCTION

The Langley Research Center of the National Aeronautics and Space Administration is a leading aerospace research center. In order to fulfill the needs of its researchers, Langley operates a number of sophisticated wind tunnels. These tunnels are used extensively and, as a consequence, have experienced numerous pressure cycles since being put into service. To insure the continued structural integrity of these tunnels, Langley has developed a comprehensive recertification program for each high-energy pressure system. One of the first facilities to be recertified under this program was the Langley 8-foot high-temperature structures tunnel. This facility is a so-called "blow-down" tunnel in which high-pressure air kept in steel storage vessels is exhausted sequentially through the air-supply piping and manifold into an air-methane gas combustor, and finally through the test chamber to the atmosphere. The highest stored-energy components of this wind tunnel are the 12 air storage vessels and the 2 methane storage vessels.

This paper describes the inspections, analyses, tests, and ASME Boiler and Pressure Vessel Code comparisons performed to recertify these vessels. In addition, this paper presents the inspection plan developed to insure continued

safe operation of these vessels. Reference 1 presents the experimental data generated for the analyses and ASME Code comparisons.

SYMBOLS

Except for the figures, this paper presents physical quantities in both the International System of Units (SI) and the U.S. Customary Units. For clarity, the figures show only SI units. All measurements and calculations were made in U.S. Customary Units. Reference 2 presents factors relating the two systems, and appendix A presents those factors used in the present investigation.

A_e	equivalent cross-sectional area
A_R	available area of reinforcement in heads of air and methane storage vessels
$A_{R,min}$	minimum required area of reinforcement for openings in shells and formed heads
a	half-length of a through flaw, or depth of a surface flaw
a_i	initial half-length of a through flaw, or initial depth of a surface flaw
C_D	drag coefficient of vessel
C_L	lift coefficient of vessel
C_{L_0}	amplitude of C_L
C_{VN}	energy absorbed in impact test on Charpy V-notch specimen
\bar{C}_{VN}	average energy absorbed in impact tests on three Charpy V-notch specimens
C_1, C_2	coefficients for fatigue-crack-growth equations
c_i	initial half-length of surface flaw
D	local inside diameter of vessel
D_{in}	inside diameter of nozzle
D_o	outside diameter of vessel
da/dN	rate of fatigue-crack growth
E	Young's modulus of elasticity
e	percent of elongation

F_{fr}	fatigue reduction factor
$F(\tau)$	aerodynamic forcing function
g	damping coefficient
g_{cr}	critical damping value
K_a	thermal conductivity of air at τ_i
K_{Ie}	experimental elastic fracture toughness
K'_{Ie}	elastic fracture toughness used in fracture-mechanics analysis
K_{max}	maximum stress-intensity factor
K_{min}	minimum stress-intensity factor
K_T	elastic stress-concentration factor for nozzle
ΔK	range of stress-intensity factor
k	spring constant of vessels
l	distance from the center line of an opening to the edge of a locally stressed area in a shell
l_e	lateral expansion obtained from impact test on Charpy V-notch specimen
M_e	elastic magnification factor on stress-intensity factor
m, n	exponents on fatigue-crack-growth equations
m_v	mass of vessel per unit length
\dot{m}	mass-flow rate
N	number of cycles
N_F	number of full pressure cycles allowed before next inspection
N_{Nu}	Nusselt number
N_{Pr}	Prandtl number
N_{Re}	Reynolds number
N_{Str}	Strouhal number
p	internal pressure

p_a	internal pressure at τ_i
p_i	internal pressure at start of tunnel run
Q	elastic shape factor for an elliptical crack
R	ratio of minimum stress to maximum stress
R_g	universal gas constant
r_{in}	inside radius
$r_{in,h}$	inside radius of spherical head of vessel
$r_{in,n}$	inside-corner radius of nozzle
$r_{in,n,min}$	minimum allowable inside-corner radius of nozzle
$r_{m,h}$	mean radius of spherical head of vessel at nozzle opening
$r_{o,n}$	outside-corner radius of nozzle
$r_{o,n,min}$	minimum allowable outside-corner radius of nozzle
S_{alt}	alternating stress intensity
$S_{\ell,m}$	local membrane stress intensity (see paragraph 4-132 of ref. 3)
$S_{\ell,m,max}$	maximum allowable value of local membrane stress intensity
S_m	design stress-intensity value
S_p	peak stress intensity (see paragraph 4-135 of ref. 3)
$S_{p,m}$	general, primary, membrane stress intensity (see paragraph 4-131 of ref. 3)
$S_{p,m,max}$	maximum allowable value of general, primary, membrane stress intensity
$S_{p,s}$	primary-plus-secondary stress intensity (see paragraph 4-134 of ref. 3)
$S_{p,s,max}$	maximum allowable value of primary-plus-secondary stress intensity
T_a	air temperature at τ_i
T_i	air temperature at start of tunnel run
t	thickness

$t_{h,min}$	minimum required thickness of spherical head of vessel (see paragraph AD-202 of ref. 3)
$t_{n,h}$	nominal thickness of spherical head of vessel at nozzle opening
U	heat-transfer coefficient
V	volume of vessel
v	average air velocity in any plane inside vessel
v_w	wind velocity
x,y	Cartesian coordinates
Y_r	ratio of outside radius to inside radius of vessel
y_o	static displacement of vessel due to lateral load
\bar{y}	amplitude of motion
\dot{y}	first derivative of y with respect to time
\ddot{y}	second derivative of y with respect to time
γ	polytropic exponent
ζ	damping ratio
μ	air viscosity at τ_i
ν	Poisson's ratio
ρ	density of air outside vessel
ρ_a	air density in vessel at τ_i
ρ_i	air density in vessel at start of tunnel run
$\sigma_{B_{max}}$	maximum bending stress on outer surface at base of vessel support skirt
$\bar{\sigma}_l$	average longitudinal stress
$\sigma_{l,in}$	longitudinal stress on inside surface
$\sigma_{l,o}$	longitudinal stress on outside surface
σ_{max}	maximum stress
σ_{min}	minimum stress

σ_r	radial stress
$\bar{\sigma}_r$	average radial stress
$\sigma_{r,in}$	radial stress on inside surface
$\sigma_{r,o}$	radial stress on outside surface
σ_t	tangential stress
$\bar{\sigma}_t$	average tangential stress
$\sigma_{t,in}$	tangential stress on inside surface
$\sigma_{t,o}$	tangential stress on outside surface
σ_u	ultimate tensile strength
$\sigma_{u,min}$	specified minimum tensile strength
σ_y	yield strength (0.2-percent offset)
$\sigma_{y,min}$	specified minimum yield strength
τ	time
τ_i	time from start of tunnel run
ϕ	phase angle by which motion lags the impressed force
ω_k	Kármán vortex frequency
ω_n	natural frequency of vessel

Abbreviations:

PT	dye-penetrant inspection
UT	ultrasonic inspection

PRESSURE-VESSEL DESCRIPTIONS

Air Storage Vessels

Figure 1 shows an aerial view of the Langley 8-foot high-temperature structures tunnel. The 12 air storage vessels of the tunnel appear in the upper right-hand quadrant of figure 1. Figure 2 shows a cross-sectional view of a typical air storage vessel. Table I presents the pertinent dimensions and characteristics of these vessels. Each vessel contains a cylindrical canister which is mounted concentric with the wall of the air storage vessel. Table II presents the pertinent dimensions and characteristics of these canisters. During

tunnel operations, the canister is designed to force the air in the vessel to flow through the 25.4-mm (1-in.) annulus between the inside wall of the pressure vessel and the outside wall of the canister. This air absorbs heat from the vessel walls while flowing along the annulus. Consequently, energy lost by the adiabatic expansion of the air is partially regained from the vessel wall. As originally constructed, each vessel also contained a horn-shaped thermal liner in the 165.1-mm (6.5-in.) nozzle. Table III gives the pertinent dimensions and characteristics of this liner. During tunnel operations, the liner protected the 165.1-mm (6.5-in.) nozzle from excessive adiabatic cooling. One end of the liner was welded to the nozzle inside-corner radius. The other end rested on a thermal liner in the air piping.

Methane Storage Vessels

The two methane storage vessels of the tunnel appear in the lower foreground of figure 1. These two vessels are similar in construction to the air storage vessels except that they contain neither canisters nor thermal liners. The canisters and liners are not needed since the methane flow rate is relatively low and little adiabatic cooling occurs. Table IV presents the pertinent dimensions and characteristics of these vessels.

RECERTIFICATION SCOPE

The recertification of the air and methane storage vessels involved the following eight basic elements:

- (1) Pressure-vessel modifications
- (2) Nondestructive examination
- (3) ASME Code comparisons
- (4) Fracture-mechanics analyses
- (5) Thermal analysis
- (6) Wind-induced vibration analysis
- (7) Determination of the operating envelopes for the air and methane storage vessels
- (8) Inspection plan

These elements were tightly interwoven; for example, inspections and analyses indicated which modifications should be performed. Conversely, new analyses and inspections were often required after modifications were completed. For clarity, each element will be discussed independently with appropriate references to interfacing elements. No attempt will be made to present the actual sequence in which recertification activities were performed.

PRESSURE-VESSEL MODIFICATIONS

A NASTRAN[®] (ref. 4) finite-element stress analysis was performed on the nozzle area of the air storage vessels. For an internal pressure of 41.4 MPa (6000 psi), this analysis indicated relatively high stresses in the welds attaching the thermal liners to the inside-corner radii of the large nozzles (fig. 3). Because of these high stresses and of the possibility that welding cracks, high residual stresses, and gouges could develop while welding the liners to the nozzles, the decision was made to remove these liners, recontour the inside-corner radii of the nozzle, and install new liners which were not attached to the nozzles.

A contour-grinding machine (fig. 4) was specially designed and fabricated at Langley to remove the original liners and recontour the inside corners of the nozzles. Figure 5 shows the nozzle region before modification.

Figure 6 shows the inside section of the liner being removed by using a cutoff wheel. Figure 7 shows the liner-support structure holding the remaining portion of the liner in place and the cutoff wheel cutting through the outside section of the liner. Figure 8 shows the liner-support structure removed and the liner being burned into pieces small enough to be removed through the nozzle. A metal shield was laid over the nozzle to protect it during this burning process. Figure 9 shows the remaining portion of the liner and its attachment weld being removed and the inside-corner radius being recontoured by using a series of grinding stones. Following this recontouring, the nozzle area was cleaned with Freon to remove all debris. Figure 10 shows the modified nozzle area with a new cylindrical thermal liner installed. After all modifications were completed, each air storage vessel was inspected and hydrotested at 1.5 times the design pressure, that is, at 62.1 MPa (9000 psi). As explained previously, the methane storage vessels contained no thermal liners. Consequently, these vessels required no modifications.

NONDESTRUCTIVE EXAMINATION

Air Storage Vessels

Large nozzles.— The following discussion lists the techniques employed in inspecting the large nozzles:

(1) Ultrasonic inspection: The configuration of these large nozzles precluded normal ultrasonic inspection. Consequently, a new test technique was developed. In this development, a full-sized mock-up of the large nozzle was fabricated. A 9.5-mm (0.375-in.) radius, semicircular slot was electrodischarge machined into the inside-corner radius of the nozzle to simulate a crack. (See fig. 11.) This is the smallest size slot which could be located repeatedly by using the techniques described herein. The slotted mock-up thus became the calibration standard for the ultrasonic inspection of the large nozzles.

A special shoe was fabricated to fit the outside-corner radius of the mock-up. A 2.25-MHz transducer having a 12.7-mm by 25.4-mm (0.5-in. by 1-in.) active area was mounted in this shoe to generate and receive shear-wave signals

in the mock-up. The shoe was fabricated to produce a sound entry angle of 22° . This entry angle permitted the sound to pass almost tangent to the inner surface of the mock-up. The practice of missing the inner surface during shear-wave inspection is not normally an accepted technique. However, by using this technique, the 9.5-mm (0.375-in.) slot in the calibration standard was located repeatedly. Consequently, this technique was used in inspecting the large nozzles. The large nozzles were ultrasonically inspected prior to the removal of the thermal liners. The nozzles on three vessels produced linear indications equal to or greater than the indications produced by the calibration standard. These three nozzles were ultrasonically reinspected following modification of the nozzles. Two of the three nozzles then gave no indications. The third produced a linear indication equal to the indication produced by the 9.5-mm (0.375-in.) slot in the mock-up.

(2) Dye-penetrant inspection: Following the modification of the nozzles, the entire inside nozzle area of each vessel was inspected by using dye-penetrant techniques. This inspection indicated no linear defects in any nozzle areas. However, nonmetallic inclusions having a width of approximately 3.6 mm (0.14 in.) were found in the nozzles of five vessels.

(3) Radiographic inspection: The modified nozzle which produced a significant ultrasonic signal was radiographically examined. This examination indicated no defects in this nozzle.

(4) Initial flaw size: From these inspections, an initial flaw depth of 9.5 mm (0.375 in.) was derived for the fracture-mechanics analysis. This 9.5-mm (0.375-in.) depth corresponds to the depth of the slot in the ultrasonic test (UT) calibration standard.

Small nozzles.- The following discussion lists the techniques employed in inspecting the small nozzles:

(1) Ultrasonic inspection: A mock-up of this small nozzle was also fabricated, and a 6.4-mm (0.25-in.) radius, semicircular slot was electrodischarge machined into the inside-corner radius of the mock-up. Another shoe was fabricated to fit the outside-corner radius of the mock-up and a 12.7-mm by 25.4-mm (0.5-in. by 1-in.) 2.25-MHz ultrasonic transducer mounted in the shoe. The same techniques used in inspecting the large nozzles of the air storage vessels were used in inspecting these nozzles. The nozzles on two vessels produced linear indications approximately equal to the indications produced by the calibration standard.

(2) Dye penetrant: The two nozzles producing linear ultrasonic indications were inspected by using dye-penetrant techniques, and no surface defects were found.

(3) Eddy current: The two nozzles producing linear ultrasonic indications were also inspected by using eddy-current techniques since these techniques indicate near-surface defects. This inspection indicated no linear defects in the nozzles.

(4) Initial flaw size: For the fracture-mechanics analysis, a flaw having a depth of 6.4 mm (0.25 in.) was assumed for these nozzles. This 6.4-mm (0.25-in.) depth corresponds to the depth of the slot in the nozzle mock-up.

Head-to-wall junctures.- The following discussion lists the techniques employed in inspecting the head-to-wall junctures:

(1) Ultrasonic inspection: The head-to-wall junctures were examined by using both longitudinal- and shear-wave techniques because there was concern that the discontinuities between layers in the vessel wall had introduced cracks into the head-to-wall juncture welds. For the longitudinal-wave examination, a mock-up of a section of this juncture was fabricated. A 4.8-mm (0.19-in.) diameter, 19.1-mm (0.75-in.) deep, flat-bottom hole was drilled into the mock-up to represent a flaw. A 2.25-MHz transducer having a 9.5-mm (0.375-in.) diameter active area was mounted in a commercial shoe and used to examine the mock-up. The signal reflected from the 4.8-mm (0.19-in.) diameter hole became the reference signal for the longitudinal-wave inspection of the head-to-wall junctures. Inspection of these junctures revealed no defects whose reflected signal exceeded the reference signal.

For the shear-wave examination, a 12.7-mm (0.5-in.) radius slot was electrodischarge machined into the mock-up to represent a crack. A 2.25-MHz transducer having a 12.7-mm by 25.4-mm (0.5-in. by 1-in.) active area was mounted in a commercial shoe for this inspection. The sound entry angle for this shoe was 45°. The signal reflected from the 12.7-mm (0.5-in.) radius slot became the reference signal for the shear-wave inspection of the junctures. Inspection of these junctures revealed no defects whose reflected signal exceeded the reference signal.

(2) Magnetic-particle inspection: The magnetic-particle inspection was performed by using handheld prods. One prod was held at the upper edge of the juncture and the other at the lower edge. The circumferential spacing between the prods was 203.2 mm to 254 mm (8 in. to 10 in.). This positioning of the prods set up a diagonal magnetic field across the juncture welds. The entire circumference of each juncture was checked at the 203.2-mm to 254-mm (8-in. to 10-in.) intervals. The magnetic-particle inspection indicated a crack that was 25.4 mm (1 in.) long by 9.5 mm (0.375 in.) deep in one of the junctures. This crack was ground out and repair welded.

(3) Initial flaw size: From these inspections, an initial-flaw depth of 12.7 mm (0.5 in.) was derived for the fracture-mechanics analysis. This 12.7-mm (0.5-in.) depth corresponds to the depth of the slot in the shear-wave calibration standard.

Canister-to-wall junctures.- The following discussion lists the techniques employed in inspecting the canister-to-wall junctures:

(1) Visual inspection: The canister-to-wall junctures were virtually inaccessible. These junctures could not be reached on the inside for ultrasonic, dye-penetrant, magnetic-particle, or eddy-current inspection. These junctures could not be ultrasonically inspected from the outside because of the multilayer construction of the vessel. Consequently, these junctures had to be visually

inspected. A flexible, fiber-optics borescope was inserted through the small upper nozzle for this inspection. This borescope had an independent cold light supply and a 35-mm camera. By using this borescope, the visual-inspection requirements of the ASME Boiler and Pressure Vessel Code (ref. 5) were met. This visual inspection indicated no cracks or weld defects in these junctures.

(2) Initial flaw size: For the fracture-mechanics analysis, a crack having a length equal to the leg length of the attachment weld, and penetrating the inner wall of the vessel, was assumed.

Hemispherical heads.- The following discussion lists the techniques employed in inspecting the hemispherical heads:

(1) Ultrasonic inspection: The hemispherical heads of the vessels were inspected by using longitudinal-wave techniques. Three vessel heads indicated areas of complete loss of back reflection during this inspection. Such loss of back reflection is unacceptable for steels in new vessels according to Section VIII, Division 2, of the ASME Boiler and Pressure Vessel Code (ref. 3). However, according to Section XI of this Code (ref. 6) such losses of back reflection are, within limits, acceptable for pressure vessels which are in service. The areas indicating complete loss of back reflection were within the limits specified in Section XI; consequently, these three vessels were judged to be safe for continued operation. No unacceptable indications were found in the remainder of the vessels.

(2) Acoustic emission: The hemispherical heads of each air storage vessel were monitored by acoustic emission sensors during hydrotesting. Eleven of the vessels were essentially quiet during the hydrotest. The twelfth vessel emitted sound from one area during the hydrotest. This area was subsequently inspected by (1) using longitudinal- and shear-wave techniques, (2) visual examination, and (3) radiographic examination. These inspections indicated no surface or subsurface flaws in the area which emitted sound. Consequently, the twelfth vessel was judged to be safe for continued operation.

Canister-to-head junctures.- The canister-to-head junctures were inspected by using the fiber-optics borescope, and no cracks or weld defects were found. No fracture-mechanics analysis was performed for this juncture because the stresses were relatively low.

Methane Storage Vessels

Large nozzles.- The following discussion lists the techniques employed in inspecting the large nozzles:

(1) Ultrasonic inspection: The shape of the large nozzles on the methane storage vessels and of the small nozzles on the air storage vessels are quite similar. Consequently, the same mock-up and test techniques were used for the ultrasonic inspection. This inspection produced no linear indications in the large nozzles of the methane storage vessels.

(2) Initial flaw size: For the fracture-mechanics analysis, a flaw having a depth of 6.4 mm (0.25 in.) was assumed for these nozzles. This 6.4-mm (0.25-in.) depth corresponds to the depth of the slot in the nozzle mock-up.

Small nozzles.- The following discussion lists the techniques employed in inspecting the small nozzles:

(1) Ultrasonic inspection: The small nozzles on the air and methane storage vessels have identical configurations. Consequently, the same shoes and techniques were used for the ultrasonic inspection. This inspection produced no linear indications in the small nozzles of the methane storage vessels.

(2) Initial flaw size: For the fracture-mechanics analysis, a flaw having a depth of 6.4 mm (0.25 in.) was assumed for these nozzles.

Head-to-wall junctures.- The head-to-wall junctures were examined by using longitudinal-wave techniques. The same procedures used in inspecting the head-to-wall junctures of the air storage vessels were used in inspecting these junctures. The longitudinal-wave inspection yielded no unacceptable indications in these junctures. These methane vessels experience very few pressure cycles relative to the air storage vessels. Consequently, no shear-wave inspection was performed on these vessels.

Hemispherical heads.- The hemispherical heads of the vessels were inspected by using longitudinal-wave techniques. This inspection yielded no unacceptable indications in these heads.

ASME CODE COMPARISONS

Although the ASME Code does not address multilayer vessels, the vessel designs were compared with the current design criteria of Section VIII, Division 2, of the 1974 ASME Boiler and Pressure Vessel Code (ref. 3). This Division of Section VIII shall be referred to hereinafter as "the Code." Such comparisons indicate whether the vessels are designed with the same factors of safety and design details as are Code-stamped vessels.

Appendix B presents the details of the ASME Code comparisons. The findings from these comparisons are listed as follows:

(1) The three steels in the air and methane storage vessels were judged to meet the Charpy impact requirements of the Code at the temperatures listed in table V(a).

(2) The three steels in the air and methane storage vessels were judged to meet Code-based drop-weight requirements at the temperatures listed in table V(b).

(3) The general, primary, membrane stress intensity $S_{p,m}$ for the cylindrical walls of the vessel slightly exceeded the maximum allowable stress intensity $S_{p,m,max}$. However, the amount by which $S_{p,m}$ exceeded $S_{p,m,max}$ was

judged to be too small to affect significantly the structural integrity of the vessels.

(4) The primary-plus-secondary stress intensity $S_{p,s}$ for the cylindrical walls of the vessels was less than the maximum allowable stress intensity $S_{p,s,max}$.

(5) For the spherical heads, the general, primary, membrane stress intensity and the primary-plus-secondary stress intensity were less than their respective allowable stress intensities.

(6) For the head-to-wall juncture, the local membrane stress intensity $S_{l,m}$ and the primary-plus-secondary stress intensity were less than their respective allowable stress intensities.

(7) For the large nozzles on the air storage vessels, the available area of reinforcement A_R was less than the minimum required area of reinforcement $A_{R,min}$. However, for these nozzles, the local membrane stress intensity and the primary-plus-secondary stress intensity were less than their respective allowable stress intensities. Since these nozzles met the Code-based requirements for both local membrane and secondary-plus-primary stress intensity, the lack of Code-level reinforcement was judged to be acceptable.

(8) For the large nozzles on the methane storage vessels, the available area of reinforcement exceeded the required minimum area of reinforcement.

(9) For the small nozzles on the air and methane storage vessels, Code paragraph AD-510 indicated that no area-reinforcement calculations needed to be made.

(10) All flanges met the Code-based requirements.

(11) The inside-corner radii on certain air and methane-storage-vessel nozzles were smaller than the minimum allowable inside-corner radii. To compensate for not meeting the Code requirements, these inside-corner radii will be carefully monitored during future inspections of selected air storage vessels (see the section of this paper entitled "Inspection Plan") to detect any flaws which might develop.

(12) Table VI shows the fatigue lives predicted for the various sections of the vessels.

FRACTURE-MECHANICS ANALYSES

Fracture-mechanics analyses were performed on the same highly stressed areas on which fatigue analyses were performed. Except for the canister-to-wall juncture which could not be fully inspected, the initial flaw depths used in these analyses came from the nondestructive examinations of the vessels. The surface length of these flaws was conservatively assumed to be 254 mm (10.0 in.). For the canister-to-wall juncture, a crack having a length equal to the leg length of the attachment weld, that is, 12.7 mm (0.50 in.), and penetrating the

inner wall of the vessel was assumed. All flaws were assumed to be oriented normal to the maximum stress direction.

Except for the upper head-to-wall and the canister-to-wall junctures, the same tangential stresses were used for the fatigue and fracture-mechanics analyses. For the two excepted junctures, the stress-concentration factors used in the fatigue analyses were deleted since the cracks were expected to propagate rapidly out of the regions affected by the stress concentrations. For surface flaws exposed to internal pressure, the maximum stress was estimated to equal the sum of the tangential stress plus the internal pressure since this pressure acts directly on the crack surfaces and forces them apart. The minimum stress for the fracture-mechanics analysis was assumed to be 0 Pa (0 ksi).

Table II in reference 1 presents the fracture-toughness data for the three steels in the air and methane storage vessels. The fracture toughness of these three steels did not decrease significantly for temperatures ranging from room temperature to about 244 K (-20° F). Consequently, single, individual values of fracture toughness were used for each steel in this temperature range. These single, individual values were slightly below the experimentally determined values of fracture toughness for the three steels (ref. 1). No analysis was required outside this temperature range.

Table III in reference 1 presents the fatigue-crack-growth data for the three steels. For the canister-to-wall juncture, an equation initially developed by Paris (ref. 7) was fitted to the upper bound of the A. O. Smith VMS 1146A data. This equation had the form

$$\frac{da}{dN} = C_1 \Delta K^n \quad (1)$$

where

$$\Delta K = K_{\max} - K_{\min} \quad (2)$$

For a through flaw in a relatively large component,

$$K_{\max} = \sigma_{\max} \sqrt{\pi a} \quad (3)$$

and

$$K_{\min} = \sigma_{\min} \sqrt{\pi a} \quad (4)$$

Equation (1) was integrated in closed form from the initial flaw size to the critical flaw size. This integration yielded a fatigue life of approximately 38 000 full pressure cycles.

For the remaining areas which were analyzed, an equation developed by Forman et al. (ref. 8) was fitted to the upper bounds of the A. O. Smith VMS 5002 and ASTM A-225 Gr.B data. This equation has the form

$$\frac{da}{dN} = \frac{C_2 \Delta K^m}{(1 - R)K_{Ie} - \Delta K} \quad (5)$$

For the surface flaws at the remaining areas in the vessels, a solution developed by Newman (ref. 9) was used to calculate stress-intensity factors. Newman's solution had the form

$$K_{\max} = \sigma_{\max} \sqrt{\frac{\pi a}{Q}} M_e \quad (6)$$

and

$$K_{\min} = \sigma_{\min} \sqrt{\frac{\pi a}{Q}} M_e \quad (7)$$

Equation (5) was numerically integrated from the initial flaw size to the critical flaw size. This integration yielded the following fatigue lives for various areas of the vessels:

Area	Approximate fatigue life, full pressure cycles, of storage vessel for -	
	Air	Methane
Large nozzle	1400	2200
Small nozzle	2200	2200
Head-to-wall juncture	10500	----

Table VII summarizes the data used in calculating these lives.

THERMAL ANALYSIS

Vessel wall temperatures were calculated for an extreme tunnel run in order to determine thermal stresses. The temperatures at various node points near the large nozzle (figs. 12 and 13) were calculated as a function of time by using the lumped-parameter, finite-difference heat-transfer program of the Martin Interactive Thermal Analysis System (ref. 10). The mass-flow rate for these calculations was assumed to be constant and equal to the maximum mass-flow rate which the vessels experience during any run. To calculate these temperatures it was necessary to obtain relationships between air properties and other parameters. The following paragraphs explain these relationships.

Time-Density Relationship

For a constant mass flow, the relationship between time and density is given by

$$\rho_a = \rho_i - \frac{\dot{m}}{V} \tau_i \quad (8)$$

Pressure and Temperature Relationships

Test data indicate that air expansion in the vessels is a polytropic process with an exponent of 1.13. For polytropic processes involving ideal gases, the relationships for pressure and temperature, respectively, are

$$p_a = p_i \left(\frac{\rho_a R_g T_i}{p_i} \right)^\gamma \quad (9)$$

and

$$T_a = T_i \left(\frac{p_a}{p_i} \right)^{\frac{\gamma-1}{\gamma}} \quad (10)$$

Viscosity-Temperature and Thermal Conductivity-Temperature Relationships

The air viscosity is assumed to be a function of temperature only and is given in SI units by

$$\mu = \frac{1.485 \times 10^{-6} T_a^{3/2}}{T_a + 111.7} \quad (11a)$$

and in U.S. Customary Units by

$$\mu = \frac{7.44 \times 10^{-7} T_a^{3/2}}{T_a + 201} \quad (11b)$$

The actual unit for T_a in equations (11) is K ($^{\circ}$ R) and for μ is kg/m-s (lbm/ft-s). The air thermal conductivity K_a is also assumed to be a function of temperature only and is given in SI units by

$$K_a = 1359\mu \quad (12a)$$

and in U.S. Customary Units by

$$K_a = 0.325\mu \quad (12b)$$

The unit for K_a in equations (12) is W/m-K (Btu/s-ft-°R).

Average Velocity as a Function of Density and of

Cross-Sectional Area of Flow

The average velocity at any plane inside the vessel was determined from the following equation which is based on one-dimensional flow:

$$v = \frac{\dot{m}}{\rho_a A_e} \quad (13)$$

The equivalent cross-sectional area A_e for nodes 1 to 5 (see fig. 12) was the mean of the cross-sectional area of (a) the annular region and (b) the circular plane which is normal to the vessel center line and contains the local inside-wall points. The equivalent cross-sectional area for nodes 6, 7, and 22 to 27 was the cross-sectional area of the flow passage at these points. (See figs. 12 and 13.)

Determination of Reynolds Number

The Reynolds number is given by the equation

$$N_{Re} = \frac{\rho_a v D}{\mu} \quad (14)$$

Heat-Transfer Coefficient Inside the Vessel

An equation developed by Bartz (ref. 11) to estimate the heat-transfer coefficients is

$$N_{Nu} = 0.026 N_{Re}^{0.8} N_{Pr}^{0.4} = \frac{UD}{K_a} \quad (15)$$

The Prandtl number N_{Pr} was assumed to be constant and equal to 0.8. The characteristic dimension used in the Nusselt number N_{Nu} and Reynolds number N_{Re} was the local inside diameter of the vessel D .

Heat-Transfer Coefficient for Outside the Vessel

The heat-transfer coefficient used for the outside of the vessel is

$$U = 22.7 \frac{W}{m^2-K} \left(U = 0.002 \frac{Btu}{s-ft^2-^{\circ}R} \right) \quad (16)$$

Table VIII presents the calculated temperatures as a function of time at the various points near the nozzle. The data in this table were used to calculate thermal stresses. These thermal stresses were used to calculate the variation of combined thermal and pressure stress with time during a tunnel run.

WIND-INDUCED VIBRATION ANALYSIS

The possible effects of wind-induced vibratory loadings on the air storage vessels were studied, and the results of this study are summarized in this section.

Problem Characterization

Researchers have long studied the oscillatory motions of isolated, slender bodies excited by aerodynamic forces. These researchers have found that when laminar flow at a low Reynolds number develops across cylinders, a so-called Kármán vortex street develops. In this street, vortices are periodically shed from alternate sides of the cylinder. This vortex shedding introduces periodic forces on the cylinder in the lift direction. In some instances, the force frequency corresponds to the natural frequency of the cylinders. In these instances, large-amplitude oscillations can develop in lightly damped structures. In addition, the vortex street from one cylinder can excite large oscillations in a downstream structure should the vortex frequency equal the natural frequency of the structure.

Analysis

References 12 and 13 indicate that no periodic vortex shedding occurs at single and at some nested cylinders for Reynolds numbers between 3.3×10^5 and 3.5×10^6 . The wind velocities corresponding to this Reynolds number range were calculated for the vessels and are listed as follows:

Reynolds number range	Corresponding wind-velocity range	Flow characteristic
3.3×10^5 to 3.5×10^6	2.7 m/s (6 mph) to 28.6 m/s (64 mph)	Turbulent

Thus, these calculations indicated no periodic vortex shedding, and, consequently, no resonant oscillations should occur for wind velocities between 2.7 and 28.6 m/s (6 and 64 mph). Although the air vessels can be excited by turbulent flow, sustained oscillations would not be expected. Also, from the data given in reference 13, the unsteady lift in the Reynolds number range from 3.3×10^5 to 3.5×10^6 appears to be wide-band random.

For wind velocities exceeding 28.6 m/s (64 mph), the vortex shedding frequency must be compared with the natural frequency of the vessel to determine whether resonance can occur. The frequency of the Kármán vortex street is given by

$$\omega_k = \frac{N_{Str} v_w}{D_o} \quad (17)$$

For wind velocities between 28.6 m/s (64 mph) and 44.7 m/s (100 mph), the maximum velocity expected at Langley, the vortex-street frequency ranges from 3.49 to 5.45 Hz. A mathematical model of the vessels was developed and the first-mode natural frequency was calculated. Field measurements were also made to determine the first-mode natural frequency and damping ratio of the vessels. The measured damping ratio and a comparison of the calculated and measured natural frequencies follow:

ω_n , Hz		ζ
Calculated	Measured	
1.67	1.51	0.012

This first-mode frequency falls below the vortex-sheet frequency range from 3.49 to 5.45 Hz. Analysis also shows that wind velocities in excess of 44.7 m/s (100 mph) are required to excite higher mode frequencies. Thus, no resonant oscillations of the vessels are expected for the wind-velocity range from 28.6 m/s (64 mph) to 44.7 m/s (100 mph).

Structural-Response Studies

As a conservative measure, it was assumed that the air vessels could be excited by regular vortex shedding. By knowing the structural frequencies, mode shapes, and damping for the vessels, the problem of steady-state response due to

a periodic forcing function was formulated. (See appendix C.) In general, this approach gives conservative results.

Aerodynamic lift coefficients used for the analysis are functions of Reynolds number and were chosen for two cases. In the first case, the stagnation pressure (i.e., $C_L = 1$) was used in developing the lateral load distribution. In the second case, a value of $C_L = 0.32$ was used, based on data given in reference 13. The latter value is more realistic and may even be slightly conservative. The load distribution assumed for the air vessels is shown in figure 14.

Based on the relationships given in appendix C, the predicted response characteristics of the air vessels alone are given in figure 14 as a function of wind velocity. Note that the peak resonant displacement (for $C_L = 1$) at the tip of the vessel is small (15.7 mm (0.62 in.)) compared with the cylinder diameter (1778 mm (70 in.)). Also, the maximum bending stress in the support skirt at resonance is low (30.4 MPa (4.4 ksi)). These relatively low displacements and stresses reflect the large-inertia and load-carrying capability of the support structure. Calculations indicate that the air vessels would remain upright in a steady 44.7-m/s (100-mph) wind because of the restoring moment due to weight. Based on this analysis, wind-induced oscillations do not appear to be a problem for the air vessels.

Steady-Wind Considerations

The support skirts for the air vessels were designed for 44.7-m/s (100-mph) winds. Calculations indicate that the air-vessel skirts can withstand much higher steady winds. (See fig. 15.) Also, the tiedown bolts and support slab were found to be more than adequate for 44.7-m/s (100-mph) winds.

Summary

The analyses presented in this section were predicated on available information on the vortex-shedding phenomenon and known structural characteristics. The problem dealt with herein is extremely complex and there are many unknown aerodynamic effects, for example, those due to geometry and wind direction. However, sufficient information was obtained for a quantitative analysis which is judged to be adequate for engineering evaluation.

DETERMINATION OF OPERATING ENVELOPES FOR THE

AIR AND METHANE STORAGE VESSELS

Operating envelopes were developed for both the static and dynamic conditions of the vessels as follows: (1) the vessels under internal pressure of 41.4 MPa (6000 psi) with no gas flow, and (2) the vessels under internal pressure less than 41.4 MPa (6000 psi) with gas flow. The discussion of these two conditions follows.

The Vessels With No Gas Flow and Pressurized to 41.4 MPa (6000 psi)

Four factors were considered in developing the operating envelope for the vessels with no gas flow and pressurized to 41.4 MPa (6000 psi). These factors were: (1) the Code, (2) the test data on the steels in the vessels, (3) the fracture-mechanics analyses, and (4) the thermal analysis.

Code paragraph AD-155 gives the minimum-service temperatures for vessels fabricated of steels like VMS 5002, VMS 1146A, and A-225 Gr.B. (The Code defines minimum-service temperature as the lowest vessel metal temperature at which full operating pressure may be applied.) This paragraph states that the minimum-service temperature for these types of steels is the temperature at which the steels meet the Charpy impact acceptance criteria of Code paragraph AM-211.1. Table V(a) presents the temperatures at which the steels were judged to meet these criteria.

Code paragraph AM-312 presents the drop-weight test requirements for certain quenched and tempered steels. These requirements do not apply to ferritic steels. However, these requirements can be applied to the vessel steels to provide an additional conservative indication of minimum allowable service temperature. Table V(b) presents the temperatures at which the steels were judged to meet these requirements.

From the section of this paper entitled "Fracture-Mechanics Analyses," the fracture toughness of the three steels was shown to be relatively constant for temperatures ranging from room temperature to 244 K (-20° F). Consequently, the cycles-to-failure values calculated for the vessels are valid for temperatures anywhere within this range. The fracture-mechanics analyses may, therefore, be considered to set a minimum temperature of 244 K (-20° F) for the vessels.

The following table summarizes the minimum temperatures for each factor considered in developing the operating envelope:

Steel	Minimum allowable temperature for factor -					
	Charpy impact		Drop weight		Fracture mechanics	
	K	°F	K	°F	K	°F
VMS 5002	255	0	255	0	244	-20
VMS 1146A	255	0	<247	<-15	244	-20
A-225 Gr.B	239	-30	247	-15	244	-20

By using the highest temperature from this table as the governing criterion, the judgment was made that the air and methane storage vessels can be safely pressurized (at 41.4 MPa (6000 psi)) down to an ambient temperature of 255 K (0° F). For an ambient temperature below 255 K (0° F), the vessels shall be depressurized.

The Vessels With Gas Flow and Pressurized to

Less Than 41.4 MPa (6000 psi)

During tunnel operations, the methane-flow rates are low and the methane storage vessels cool a negligible amount. Since little cooling occurs, the methane storage vessels were judged to be safe for flow operations down to 225 K (0° F).

The section of this paper entitled "Thermal Analysis" showed that the air storage vessels can cool significantly during tunnel operations. That section showed that after an extreme, 2-minute tunnel run, the inside-surface temperatures of the large nozzles can drop as much as 11 K (20° F). However, the outside-surface temperatures of the nozzles are virtually unchanged after the 2-minute run.

The following rationale was developed to govern the air-storage-vessel operations during such tunnel runs:

(1) During tunnel runs, the inside-wall temperature shall be allowed to drop below 255 K (0° F). This allowance is believed reasonable since analysis showed that the combined pressure and thermal stress on the inside wall continuously decreases during a tunnel run.

(2) The temperature at the tip of an assumed critical-length crack shall not be allowed to drop below 255 K (0° F) during a tunnel run. This allowance is judged to be reasonable since test data (ref. 1) showed that the fracture toughness of the steels did not vary significantly with temperature down to 244 K (-20° F).

Analysis showed that for an extreme, 2-minute tunnel run, the temperature at the tip of a critical-length crack can drop as much as 7 K (13° F). By considering the results of this analysis and the rationale developed for the air storage vessels, the following operating restrictions were adopted for the Langley 8-foot high-temperature structures tunnel:

(1) For ambient temperatures greater than 267 K (20° F), the air vessels may be blown down without restriction.

(2) For ambient temperatures less than or equal to 267 K (20° F), the air vessels may not be blown down for research projects. This 267 K (20° F) restriction will assure that the temperature at the tip of a critical-length crack will never drop below 255 K (0° F).

Thermal Enclosure

Figure 16 shows a thermal enclosure which, as a result of this recertification, has been built around the air storage vessels. The temperature inside this enclosure will always be kept above 267 K (20° F) so that the air storage vessels will always be available for research operations.

INSPECTION PLAN

Table IX presents the inspection plan for the air and methane storage vessels. These inspections are briefly described as follows:

(1) The large and small nozzles will be inspected every 5 years by using UT-shear-wave techniques. In addition, the one large and two small nozzles which produced linear indications during UT inspection will be inspected by using PT techniques.

(2) The head-to-wall juncture will be inspected every 10 years by using UT-shear-wave techniques.

(3) The canister-to-wall junctures on two, preselected air storage vessels will be visually inspected every 5 years by using a fiber-optics borescope.

(4) The three hemispherical heads which had indications of complete loss of back reflection shall be inspected at a decreasing frequency by using UT-longitudinal-wave techniques. All delaminations located during this inspection will be outlined with paint. Subsequent inspection will indicate whether further delamination is occurring.

CONCLUDING REMARKS

Twelve air storage vessels and two methane storage vessels at the Langley Research Center of the National Aeronautics and Space Administration were recently recertified. This recertification involved (a) modification of the vessels to remove highly stressed welds; (b) hydrotesting of the modified vessels; (c) inspection of the vessels; (d) repair of all relevant defects located during the inspection; (e) comparison of the vessel designs with the design criteria of Section VIII, Division 2, of the 1974 ASME Boiler and Pressure Vessel Code; (f) fracture-mechanics, thermal, and wind-induced vibration analyses of the vessels; and (g) development of operating envelopes and a future inspection plan for the vessels. Following these modifications, analyses, and tests, the vessels were recertified for operation at full design pressure (41.4 MPa (6000 psi)) within the operating envelope developed.

Langley Research Center
National Aeronautics and Space Administration
Hampton, VA 23665
November 9, 1976

APPENDIX A

CONVERSION OF SI UNITS TO U.S. CUSTOMARY UNITS

The International System of Units (SI) was adopted by the Eleventh General Conference on Weights and Measures held in Paris in 1960 (ref. 2). Conversion factors required for units used herein are given in the following table:

Physical quantity	SI Unit	Conversion factor	U.S. Customary Unit
Force	newton (N)	0.2248	lbf
Length	meter (m)	0.3937×10^2	in.
Stress	pascal (Pa)	0.145×10^{-6}	ksi
Frequency	hertz (Hz)	60	cpm
Temperature	kelvin (K)	$\frac{9}{5} K - 459.7$	°F
Mass	kilogram (kg)	2.205	lbm

Prefixes and symbols to indicate multiples of units are as follows:

Multiple	Prefix	Symbol
10^{-3}	milli	m
10^6	mega	M
10^9	giga	G

APPENDIX B

ASME CODE COMPARISONS

The designs of the vessels were compared with the design criteria of Section VIII, Division 2, of the 1974 ASME Boiler and Pressure Vessel Code (ref. 3). This appendix presents the details of these comparisons.

The Code lists numerous alternative requirements and exceptions to its requirements. For clarity, only the requirements used in analyzing the vessels shall be addressed herein.

Materials

Tensile and chemical properties.— No test material was available from the original VMS 5002, VMS 1146A, and ASTM A-225 Gr.B steels used for construction. Consequently, new material was procured for testing. Table X shows a comparison between the tensile and chemical properties of the new steels tested (ref. 1) and the properties (from the original data sheets) of the steels in the air and fuel storage vessels. Generally, the properties of the steels tested matched those of the steels in the vessels quite well. Table X also shows the specified minimum tensile strengths for the three steels. The ultimate tensile strength of the VMS 1146A tested was slightly below the specified minimum tensile strength. However, this slight difference was not expected to affect the test results significantly. Of the three steels in the pressure vessel, only the A-225 Gr.B is Code approved (ref. 3).

Charpy V-notch impact properties.— Table AM-211.1 of the Code (ref. 3) presents the minimum Charpy V-notch impact requirements for carbon and low-alloy steels (such as VMS 5002, VMS 1146A, and A-225 Gr.B). Comparison of table AM-211.1 with table X of this report yields the following impact requirements for the three steels:

Steel	Specified minimum tensile strength		Required C_{VN} or l_e at minimum service temperature
	MPa	ksi	
VMS 5002	641	93	Average for three specimens; $\bar{C}_{VN} \geq 27.1 \text{ N-m (20 ft-lb)}$ Minimum for one specimen; $C_{VN} \geq 20.3 \text{ N-m (15 ft-lb)}$
VMS 1146A	724	105	Minimum for three specimens; $l_e \geq 0.38 \text{ mm (0.015 in.)}$
A-225 Gr.B	517	75	Average for three specimens; $\bar{C}_{VN} \geq 20.3 \text{ N-m (15 ft-lb)}$ Minimum for one specimen; $C_{VN} = 16.3 \text{ N-m (12 ft-lb)}$

APPENDIX B

Table V of reference 1 presents the Charpy impact results for VMS 5002. The C_{VN} at 255 K (0° F) is 22 N-m (16 ft-lbf) and at 244 K (-20° F) is 34 N-m (25 ft-lbf). The data point from 244 K (-20° F) can be translated to 255 K (0° F) to give an average C_{VN} of 28 N-m (20.5 ft-lbf) and a minimum C_{VN} of 22 N-m (16 ft-lbf) at 255 K (0° F). These average and minimum values exceed the impact requirements in the preceding table. The average C_{VN} is based on two rather than three specimens. However, the conservative practice of translating the data point from 244 K (-20° F) to 255 K (0° F) is judged to compensate for the lack of one data point in calculating the average C_{VN} . Thus, the C_{VN} data are judged to show that the VMS 5002 steel meets the Code impact requirements at 255 K (0° F).

Table V of reference 1 also presents the Charpy impact results for VMS 1146A. The l_e at 255 K (0° F) is 0.53 mm (0.021 in.) and at 244 K (-20° F) is 0.69 mm (0.027 in.). If the data point at 244 K (-20° F) is translated to 255 K (0° F), the average l_e is 0.61 mm (0.024 in.) which exceeds the impact requirements in the preceding table. This average l_e value is also based on two rather than three specimens, but again the conservative practice of translating the data point at 244 K (-20° F) to 255 K (0° F) is judged to compensate for the lack of one data point. Thus, the l_e data on VMS 1146A are judged to meet the Code impact requirements at 255 K (0° F).

Table V of reference 1 also presents the Charpy impact results for A-225 Gr.B. The data points from 228 K (-50° F) and 233 K (-40° F) can be translated to 239 K (-30° F) to give an average C_{VN} of 28 N-m (21 ft-lbf) and a minimum C_{VN} of 27 N-m (20 ft-lbf). These average and minimum values exceed the impact requirements in the preceding table. Thus, A-225 Gr.B meets the impact requirements of the Code at 239 K (-30° F).

Drop-weight requirements.— Code paragraph AM-312 (ref. 3) presents the drop-weight test requirements for certain quenched and tempered steels. Paragraph AM-312 requires that both of two test specimens meet the "no-break" criterion at the minimum service temperature. The VMS 5002, VMS 1146A, and A-225 Gr.B materials are not quenched and tempered steels; consequently, paragraph AM-312 would not apply. Nevertheless, this criterion can be applied to these steels to provide an additional conservative indication of the minimum allowable service temperature for the three steels. Table VI of reference 1 presents the results of the drop-weight tests on the VMS 5002 and A-225 Gr.B specimens. Three VMS 5002 specimens met the "no-break" criterion at 255 K (0° F), and two A-225 Gr.B specimens met the "no-break" criterion at 247 K (-15° F). Thus, by using the criterion of paragraph AM-312, VMS 5002 may be used in service at 255 K (0° F) and A-225 Gr.B may be used at 247 K (-15° F).

A lack of material precluded drop-weight testing the VMS 1146A. However, for temperatures above 239 K (-30° F), the VMS 1146A absorbed the highest energies in the Charpy impact tests. (See table V of ref. 1.) Consequently, VMS 1146A would be expected to meet the "no-break" criterion at even lower temperatures in a drop-weight test (which is also an impact test) than either VMS 5002 or A-225 Gr.B.

APPENDIX B

Code Design Comparisons

Code appendix 1 (ref. 3) presents the basis for establishing design stress-intensity values. If the governing Code basis, that is,

$$S_m = \frac{1}{3} \sigma_{u,min} \quad (B1)$$

is applied to the vessel head, shell, and nozzle materials, the S_m values in table XI result. Table X presents the $\sigma_{u,min}$ values for the three steels.

Cylindrical walls away from head juncture.— Code paragraph 4-222(a) presents the equation for the general, primary, membrane stress intensity in a pressurized cylindrical shell. This equation has the form

$$S_{p,m} = \frac{pr_{in}}{t} + \frac{p}{2} \quad (B2)$$

Code paragraph 4-222(b) presents the equation for the maximum value of the primary-plus-secondary stress intensity in a pressurized cylindrical shell. This equation has the form

$$S_{p,s} = 2p \frac{Y_r^2}{Y_r^2 - 1} \quad (B3)$$

Consider first the air storage vessels. Substituting into equation (B2) from table I yields

$$S_{p,m} = 249 \text{ MPa (36.1 ksi)} \quad (B4)$$

Table XII presents the maximum allowable value of the general, primary, membrane stress intensity for VMS 1146A,

$$S_{p,m,max} = 241 \text{ MPa (35.0 ksi)} \quad (B5)$$

Thus,

$$S_{p,m} > S_{p,m,max} \quad (B6)$$

and the cylindrical walls of the air storage vessels are overstressed according to the Code.

Substituting values from table I into equation (B3) yields

$$S_{p,s} = 290 \text{ MPa (42.0 ksi)} \quad (B7)$$

APPENDIX B

Table XII also presents the maximum allowable value of the primary-plus-secondary stress intensity for VMS 1146A as

$$S_{p,s,max} = 724 \text{ MPa (105 ksi)} \quad (B8)$$

Thus, the primary-plus-secondary stress-intensity requirement of the Code is met.

Consider next the methane storage vessels. Substituting values from table IV into equation (B2) yields

$$S_{p,m} = 257 \text{ MPa (37.3 ksi)} \quad (B9)$$

From table XII for VMS 1146A,

$$S_{p,m,max} = 241 \text{ MPa (35.0 ksi)} \quad (B10)$$

and

$$S_{p,m} > S_{p,m,max} \quad (B11)$$

Thus, the cylindrical walls of the methane storage vessels are also slightly overstressed according to the Code.

Substitution of values from table IV into equation (B3) yields

$$S_{p,s} = 301 \text{ MPa (43.6 ksi)} \quad (B12)$$

From table XII for VMS 1146A,

$$S_{p,s,max} = 724 \text{ MPa (105.0 ksi)} \quad (B13)$$

Thus, the primary-plus-secondary stress-intensity requirement of the Code is met.

For both the air and methane storage vessels, the amount by which $S_{p,m}$ exceeds $S_{p,m,max}$ is judged to be too small to affect the structural integrity of the vessels significantly.

Spherical head away from wall juncture and nozzles.— Code paragraph 4-322(a) presents the equation for the general, primary, membrane stress intensity in a pressurized spherical shell. This equation has the form

APPENDIX B

$$S_{p,m} = 0.75p \frac{Y_r^3 + 1}{Y_r^3 - 1} \quad (B14)$$

Code paragraph 4-322(b) presents the equation for the maximum value of the primary-plus-secondary stress intensity in a pressurized spherical shell. This equation has the form

$$S_{p,s} = 1.5p \frac{Y_r^3}{Y_r^3 - 1} \quad (B15)$$

Comparison of tables I and IV indicates that the p and Y_r values for the air and methane storage vessels are the same. Consequently, one set of calculations is valid for both types of vessels.

Substitution of values from table I into equation (B14) yields

$$S_{p,m} = 155 \text{ MPa (22.5 ksi)} \quad (B16)$$

As before, the allowable value of $S_{p,m}$ is $S_{p,m,max}$. From table XII for A-225 Gr.B,

$$S_{p,m,max} = 172 \text{ MPa (25 ksi)} \quad (B17)$$

Thus, the spherical heads of the air and methane storage vessels meet the general, primary, membrane stress-intensity requirement of the Code.

Substituting values from table I into equation (B15) yields

$$S_{p,s} = 186 \text{ MPa (27.0 ksi)} \quad (B18)$$

As before, the allowable value of $S_{p,s}$ is $S_{p,s,max}$. From table XII for A-225 Gr.B,

$$S_{p,s,max} = 517 \text{ MPa (75.0 ksi)} \quad (B19)$$

Thus, the spherical heads of the air and methane storage vessels meet the primary-plus-secondary stress-intensity requirement of the Code.

Head-to-wall junctures.— The stresses at the head-to-wall junctures, which were calculated by using a discontinuity analysis consistent with the procedures

APPENDIX B

outlined in Code article 4-7, are listed in table XIII. (In calculating these stresses, E and ν were assumed to equal 207 GPa (30×10^3 ksi) and 0.3, respectively.)

Consider first the wall stresses at the juncture. Code paragraph 4-132 states that the local membrane stress intensity $S_{l,m}$ is derived from the average values of the stresses across the vessel thickness. (These stresses include stresses due to design pressure and specified mechanical loads, but exclude all thermal and peak stresses.) From table XIII, the average values of the stresses at the juncture are

$$\bar{\sigma}_t = \frac{\sigma_{t,o} + \sigma_{t,in}}{2} = 181 \text{ MPa (26.3 ksi)} \quad (B20)$$

$$\bar{\sigma}_l = \frac{\sigma_{l,o} + \sigma_{l,in}}{2} = 105 \text{ MPa (15.2 ksi)} \quad (B21)$$

$$\bar{\sigma}_r = \frac{\sigma_{r,o} + \sigma_{r,in}}{2} = -21 \text{ MPa (-3 ksi)} \quad (B22)$$

The local membrane stress intensity $S_{l,m}$ is given by

$$S_{l,m} = \bar{\sigma}_t - \bar{\sigma}_r = 183 - (-21) = 204 \text{ MPa (29.6 ksi)} \quad (B23)$$

Table XII presents the maximum allowable value of the local membrane stress intensity for VMS 1146A as

$$S_{l,m,max} = 362 \text{ MPa (52.5 ksi)} \quad (B24)$$

Thus, the local membrane stress-intensity requirement of the Code for the wall is met at the juncture.

Code paragraph 4-134 states that the primary-plus-secondary stress intensity $S_{p,s}$ is derived from the highest value of the combined, local, primary membrane stresses, the primary bending stresses, and the secondary stresses. (These combined stresses include stresses due to design pressure, certain specified mechanical loads, general thermal gradients, and gross structural discontinuities.) Table XIII gives these stresses at the juncture. Analysis of this table indicates that the highest value of $S_{p,s}$ occurs at the inside surface of the wall. This highest value is given by

$$S_{p,s} = \sigma_{t,in} - \sigma_{r,in} = 251 \text{ MPa (36.4 ksi)} \quad (B25)$$

APPENDIX B

From table XII for VMS 1146A,

$$S_{p,s,max} = 724 \text{ MPa (105 ksi)} \quad (B26)$$

Thus, the primary-plus-secondary stress-intensity requirement of the Code for the wall is met at the juncture.

Next, consider the head stresses at the juncture. From table XIII, the average values of the head stresses at the juncture are

$$\bar{\sigma}_t = \frac{\sigma_{t,o} + \sigma_{t,in}}{2} = 192 \text{ MPa (27.9 ksi)} \quad (B27)$$

$$\bar{\sigma}_l = \frac{\sigma_{l,o} + \sigma_{l,in}}{2} = 123 \text{ MPa (17.8 ksi)} \quad (B28)$$

$$\bar{\sigma}_r = \frac{\sigma_{r,o} + \sigma_{r,in}}{2} = -21 \text{ MPa (-3 ksi)} \quad (B29)$$

The local membrane stress intensity $S_{l,m}$ is given by

$$S_{l,m} = \bar{\sigma}_t - \bar{\sigma}_r = 192 - (-21) = 213 \text{ MPa (30.9 ksi)} \quad (B30)$$

From table XII for A-225 Gr.B,

$$S_{l,m,max} = 259 \text{ MPa (37.5 ksi)} \quad (B31)$$

Thus, the local membrane stress-intensity requirement of the Code for the head is met at the juncture.

Analysis of table XIII indicates that the highest value of $S_{p,s}$ occurs at the inside surface of the head. This highest value is given by

$$S_{p,s} = \sigma_{t,in} - \sigma_{r,in} = 201 - (-41) = 242 \text{ MPa (35.1 ksi)} \quad (B32)$$

From table XII for A-225 Gr.B,

$$S_{p,s,max} = 517 \text{ MPa (75 ksi)} \quad (B33)$$

APPENDIX B

Thus, the primary-plus-secondary stress-intensity requirement for the head is met at the juncture.

Area of reinforcement for nozzles.— Code paragraph AD-520(a) presents the equation for calculating the area of reinforcement required for openings in internally pressurized shells and formed heads. This equation is

$$A_{R,min} = D_{in} t_{h,min} F \quad (B34)$$

where $F = 1$ for the nozzles in the air and methane storage vessels. Therefore,

$$A_{R,min} = D_{in} t_{h,min} \quad (B35)$$

Consider, first, the large nozzle on the air storage vessel. From table I,

$$D_{in} = 165 \text{ mm (6.5 in.)} \quad (B36)$$

Code paragraph AD-202(a) presents the equation for the required head thickness

$$t_{h,min} = \frac{0.5 p r_{in,h}}{S_m - 0.25 p} \quad (B37)$$

By substituting values from table I,

$$t_{h,min} = 97 \text{ mm (3.83 in.)} \quad (B38)$$

Thus,

$$A_{R,min} = D_{in} t_{h,min} = 0.0161 \text{ m}^2 \text{ (24.9 in}^2\text{)} \quad (B39)$$

A graphical solution for the available area of reinforcement A_R was performed while observing the limits of reinforcement specified in code paragraph AD-540. This solution showed

$$A_R = 0.0137 \text{ m}^2 \text{ (21.2 in}^2\text{)} \quad (B40)$$

APPENDIX B

Because the Code requirement for area reinforcement was not met, the tangential stresses in the modified nozzle area were interpolated from the results of the finite-element stresses analysis on the original nozzle (fig. 3). Figure 17 shows these interpolated stresses and indicates that the average tangential stress is approximately

$$\bar{\sigma}_t = 241 \text{ MPa (35 ksi)} \quad (\text{B41})$$

The average radial stress is due to internal pressure and is given by

$$\bar{\sigma}_r = \frac{-41 + 0}{2} = -21 \text{ MPa (-3 ksi)} \quad (\text{B42})$$

The local membrane stress intensity $S_{\ell,m}$ is given by

$$S_{\ell,m} = \bar{\sigma}_t - \bar{\sigma}_r = 262 \text{ MPa (38 ksi)} \quad (\text{B43})$$

From table XII for VMS 5002,

$$S_{\ell,m,\max} = 321 \text{ MPa (46.5 ksi)} \quad (\text{B44})$$

Thus, the local membrane stress-intensity requirement of the Code for the large nozzle is met.

Analysis of figure 17 shows that the maximum tangential stress occurs at the inside surface and is approximately

$$\sigma_{t,\text{in}} = 303 \text{ MPa (44 ksi)} \quad (\text{B45})$$

The maximum radial stress, which is due to the internal pressure, also occurs at the inside surface and is given by

$$\sigma_{r,\text{in}} = -41 \text{ MPa (-6 ksi)} \quad (\text{B46})$$

For the large nozzle, the peak stress intensity is given by

$$S_p = \sigma_{t,\text{in}} - \sigma_{r,\text{in}} = 345 \text{ MPa (50 ksi)} \quad (\text{B47})$$

APPENDIX B

This peak stress intensity can be used as a conservative estimate of $S_{p,s}$ since, by definition (see Code fig. 4-130.1),

$$S_p \geq S_{p,s} \quad (B48)$$

It was assumed, therefore, that

$$S_{p,s} = S_p = 345 \text{ MPa (50 ksi)} \quad (B49)$$

From table XII for VMS 5002,

$$S_{p,s,max} = 641 \text{ MPa (93 ksi)} \quad (B50)$$

Thus, the large nozzle also meets the primary-plus-secondary stress-intensity requirement of the Code. Since the large nozzles on the air storage vessels met the Code requirements for both local membrane stress intensity and primary-plus-secondary stress intensity, the lack of Code-required area reinforcement was judged not to compromise the structural integrity of the vessels.

Consider next the large nozzle on the methane storage vessel. From table IV,

$$D_{in} = 81.3 \text{ mm (3.2 in.)} \quad (B51)$$

By use of equation (B38) of this report,

$$A_{R,min} = D_{in} t_{h,min} = 0.0079 \text{ m}^2 (12.3 \text{ in}^2) \quad (B52)$$

A graphical solution for the available area of reinforcement showed

$$A_R = 0.0145 \text{ m}^2 (22.44 \text{ in}^2) \quad (B53)$$

and that all of the other requirements of Code paragraphs AD-501 through AD-550 were met.

Consider next the small nozzles on the air and methane storage vessels. Code paragraph AD-510 presents the requirements for circular openings not requiring reinforcement. For the air and fuel storage vessels, reinforcement is not required if

APPENDIX B

$$D_{in} < 0.2 \sqrt{r_{m,h} t_{n,h}} \quad (B54)$$

and

$$\ell > 2.5 \sqrt{r_{m,h} t_{n,h}} \quad (B55)$$

From tables I and IV,

$$D_{in} = 50.8 \text{ mm (2.0 in.)} \quad (B56)$$

Substituting into the right side of inequality (B54) gives

$$0.2 \sqrt{r_{m,h} t_{n,h}} = 61.0 \text{ mm (2.4 in.)} \quad (B57)$$

Thus,

$$D_{in} < 0.2 \sqrt{r_{m,h} t_{n,h}} \quad (B58)$$

The minimum value of ℓ is given by

$$\ell = \frac{\pi r_{in,h}}{2} = 1.20 \text{ m (47.1 in.)} \quad (B59)$$

Substituting into the right side of inequality (B55) gives

$$2.5 \sqrt{r_{m,h} t_{n,h}} = 762 \text{ mm (30.0 in.)} \quad (B60)$$

Thus,

$$\ell > 2.5 \sqrt{r_{m,h} t_{n,h}} \quad (B61)$$

Consequently, the requirements of Code paragraph AD-510 are met, and there is no requirement for reinforcement of the small nozzles.

Flanges.— Code paragraph AD-711 states that flanges conforming to USAS B16.5-1968 on steel pipe flanges and flanged fittings (ref. 14) are acceptable. It is stated by USAS B16.5-1968 (ref. 14) that, for temperatures between 244 K (-20° F) and 311 K (100° F), Class 2500 flanges made of carbon or low-alloy steels may be used at pressures up to 41.4 MPa (6000 psi).

All flanges on the air and methane storage vessels are Class 2500 flanges. Consequently, these flanges may be used at pressures up to 41.4 MPa (6000 psi) (the design pressure for the vessels; see tables I and IV) and meet the Code requirements for flanges.

APPENDIX B

Nozzle corner-radius requirements.- Code figure AD-613.1 gives the minimum allowable inside- and outside-corner radii for nozzles:

$$r_{in,n,min} = 19.1 \text{ mm (0.75 in.)} \quad (B62)$$

$$r_{o,n,min} = 6.4 \text{ mm (0.25 in.)} \quad (B63)$$

For the large nozzle of the air storage vessels, table I shows

$$r_{in,n} = 50.8 \text{ mm (2.0 in.)} > r_{in,n,min} \quad (B64)$$

$$r_{o,n} = 38.1 \text{ mm (1.5 in.)} > r_{o,n,min} \quad (B65)$$

Thus, the large nozzles of the air storage vessels meet the Code requirement.

For the large nozzles of the methane storage vessels, table IV shows

$$r_{in,n} = 6.4 \text{ mm (0.25 in.)} < r_{in,n,min} \quad (B66)$$

$$r_{o,n} = 12.7 \text{ mm (0.50 in.)} > r_{o,n,min} \quad (B67)$$

Thus, the large nozzles of the methane storage vessels do not meet the Code requirements.

For the small nozzles on the air and methane storage vessels, tables I and IV show

$$r_{in,n} = 6.4 \text{ mm (0.25 in.)} < r_{in,n,min} \quad (B68)$$

$$r_{o,n} = 12.7 \text{ mm (0.50 in.)} > r_{o,n,min} \quad (B69)$$

Thus, the small nozzles of the air and methane storage vessels do not meet the Code requirement for inside-corner radii. To compensate for not meeting the Code, inside-corner radii will be carefully monitored during future inspections of selected air storage vessels (see table IX) to detect any flaws which may develop.

Fatigue analyses.- Code Article 5-1 outlines the procedures for performing a fatigue analysis on pressure vessels. The following areas were selected for fatigue analysis because of the relatively high stresses present:

APPENDIX B

- (1) The large nozzle on the air storage vessel
- (2) The large nozzle on the methane storage vessel
- (3) The small nozzles on the air and methane storage vessels
- (4) The lower head-to-wall juncture on the air storage vessel
- (5) The upper head-to-wall juncture on the air storage vessel
- (6) The upper canister-to-wall juncture

(1) The large nozzle on the air storage vessel: From equation (B47) of this report,

$$S_p = 345 \text{ MPa (50 ksi)}$$

for the large nozzle when the internal pressure is 41.4 MPa (6000 psi). For a full pressure cycle, that is, 0 MPa to 41.4 MPa (6000 psi) to 0 MPa, Code paragraph 5-110.3(3) indicates that the alternating stress intensity is given by

$$S_{alt} = 0.5S_p = 173 \text{ MPa (25 ksi)} \quad (\text{B70})$$

By entering the Code S-N curve for carbon and low-alloy steels (Code fig. 5-110.1) with this value of S_{alt} , a fatigue life of approximately 50 000 full pressure cycles is obtained.

(2) The large nozzle on the methane storage vessel: The procedures outlined in reference 15 were used to calculate the stress-concentration factor for this nozzle. These procedures indicated

$$K_T \approx 2.1 \quad (\text{B71})$$

This stress-concentration factor compares favorably with the stress indices for nozzles given in Code paragraph 4-612(a). Because of this favorable comparison, the stress indices given in Code paragraph 4-612(a) were assumed to apply.

From equation (B16) of this report,

$$S_{p,m} = 155 \text{ MPa (22.5 ksi)}$$

for a pressure of 41.4 MPa (6000 psi). By applying the inside-corner stress index from Code paragraph 4-612(a),

APPENDIX B

$$S_p = 2.2S_{p,m} = 341 \text{ MPa (49.5 ksi)} \quad (\text{B72})$$

For a full pressure cycle,

$$S_{alt} = 0.5S_p = 171 \text{ MPa (24.8 ksi)} \quad (\text{B73})$$

By entering Code figure 5-110.1 with this value of S_{alt} , a fatigue life of approximately 50 000 full pressure cycles is obtained.

(3) The small nozzles on the air and methane storage vessels: The procedures outlined in reference 15 were also used to calculate the stress-concentration factor for these nozzles. These procedures indicated that

$$K_T = 1.8 \quad (\text{B74})$$

Again, because of the favorable comparison between this stress-concentration factor and the stress indices in Code paragraph 4-612(a), the Code indices were assumed to apply. By using these indices and the $S_{p,m}$ value from equation (B16), a fatigue life of approximately 50 000 full pressure cycles is obtained for these nozzles.

(4) The lower head-to-wall juncture on the air storage vessel: For an internal pressure of 41.4 MPa (6000 psi), figure 18 shows the tangential stresses calculated in a NASTRAN® (ref. 4) finite-element stress analysis of the head-to-wall juncture. From figure 18, on the inside surface of the juncture,

$$\sigma_{t,in} = 181 \text{ MPa (26.3 ksi)} \quad (\text{B75})$$

From the internal pressure on the inside surface of the juncture,

$$\sigma_{r,in} = -41 \text{ MPa (-6 ksi)} \quad (\text{B76})$$

Inspection of figure 18 indicates that the peak stress intensity at the head-to-wall juncture is given by

$$S_p = \sigma_{t,in} - \sigma_{r,in} = 222 \text{ MPa (32.2 ksi)} \quad (\text{B77})$$

APPENDIX B

From Code paragraph 5-110.3(3), for a full pressure cycle,

$$S_{alt} = 0.5S_p = 111 \text{ MPa (16.1 ksi)} \quad (B78)$$

From Code figure 5-110.1, a fatigue life of approximately 380 000 full pressure cycles is obtained for this S_{alt} .

(5) The upper head-to-wall juncture on the air storage vessel: The upper juncture contains a backing strip. Code paragraph AD-412.1 states that stress-concentration factors of 2 shall be applied when such backing strips are left in place. Applying these stress-concentration factors to the stresses on the inside surface of the juncture (fig. 18) yields

$$\sigma_{t,in} = 362 \text{ MPa (52.5 ksi)} \quad (B79)$$

and

$$\sigma_{r,in} = -82 \text{ MPa (-11.9 ksi)} \quad (B80)$$

Thus, for a full pressure cycle,

$$S_p = \sigma_{t,in} - \sigma_{r,in} = 444 \text{ MPa (64.4 ksi)} \quad (B81)$$

and

$$S_{alt} = 0.5S_p = 222 \text{ MPa (32.2 ksi)} \quad (B82)$$

From Code figure 5-110.1, a fatigue life of approximately 23 000 full pressure cycles is obtained for this S_{alt} .

(6) The upper canister-to-wall juncture: For a pressure of 41.4 MPa (6000 psi), figure 18 also shows the tangential stresses calculated for the canister-to-wall juncture. From figure 18, on the inside surface of the juncture,

$$\sigma_{t,in} = 188 \text{ MPa (27.3 ksi)} \quad (B83)$$

From the internal pressure, on the inside surface of the juncture,

$$\sigma_{r,in} = -41 \text{ MPa (-6 ksi)} \quad (B84)$$

APPENDIX B

Inspection of figure 18 indicates that the peak stress intensity at the canister-to-wall juncture is given by

$$S_p = \sigma_{t,in} - \sigma_{r,in} = 231 \text{ MPa (33.5 ksi)} \quad (\text{B85})$$

The upper canister-to-wall juncture is made by using fillet welds. Code paragraph 5-112 specifies that a fatigue reduction factor of 4 must be used for fillet-welded attachments. Applying this fatigue reduction factor F_{fr} to S_p yields

$$F_{fr}S_p = 919 \text{ MPa (133.2 ksi)} \quad (\text{B86})$$

The S_{alt} for a full pressure cycle is given by

$$S_{alt} = 0.5F_{fr}S_p = 460 \text{ MPa (66.6 ksi)} \quad (\text{B87})$$

From Code figure 5-110.1, a fatigue life of approximately 1700 cycles is obtained for this S_{alt} .

APPENDIX C

MATHEMATICAL CHARACTERIZATION OF STEADY-STATE RESPONSE OF THE AIR STORAGE VESSELS OF THE LANGLEY 8-FOOT HIGH-TEMPERATURE STRUCTURES TUNNEL

Consider a two-dimensional cylinder of unit length as shown in figure 14. The equation of motion of a cylinder in a flow is characterized by

$$\ddot{y} + 2\zeta\omega_n\dot{y} + \omega_n^2 y = \frac{1}{m_v} F(\tau) \quad (C1)$$

where m_v is the mass of the cylinder (per unit length). The natural frequency of the cylinder is given by

$$\omega_n^2 = \frac{k}{m_v}$$

and the damping ratio is given by

$$\zeta = \frac{g}{g_{cr}}$$

It should be noted that the chosen form of the damping mechanism is based on the premise of harmonic motion with emphasis on solutions at resonance. Total damping is made of both air resistance and structural damping. Also, the aerodynamic forcing function in the lateral direction (normal to the wind) is given by

$$F(\tau) = \frac{1}{2} \rho v_w^2 C_L D_o \quad (C2)$$

The lift coefficient C_L excited by the shedding of vortices is assumed to be of the form

$$C_L = C_{L_o} e^{i\omega_k \tau} \quad (C3)$$

Substituting equations (C2) and (C3) into equation (C1) yields

$$\ddot{y} + 2\zeta\omega_n\dot{y} + \omega_n^2 y = \frac{1}{2m_v} \rho v_w^2 C_{L_o} D_o e^{i\omega_k \tau} \quad (C4)$$

APPENDIX C

The steady-state solution of equation (C4) is given by $\left(\text{for } y = \bar{y} e^{i(\omega_k \tau - \phi)} \right)$

$$y(t) = \frac{\rho D_o C_{L_o}}{2m_v \omega_n^2} \frac{v_w^2 e^{i(\omega_k \tau - \phi)}}{\left\{ \left[1 - \left(\frac{\omega_k}{\omega_n} \right)^2 \right]^2 + \left(2\zeta \frac{\omega_k}{\omega_n} \right)^2 \right\}^{1/2}} \quad (C5)$$

where the amplitude of motion is given by

$$\bar{y} = \frac{\rho D_o C_{L_o} v_w^2}{2m_v \omega_n^2} \frac{1}{\left\{ \left[1 - \left(\frac{\omega_k}{\omega_n} \right)^2 \right]^2 + \left(2\zeta \frac{\omega_k}{\omega_n} \right)^2 \right\}^{1/2}} \quad (C6)$$

Equation (C6) can be nondimensionalized by dividing by the zero frequency (static) displacement of the cylinder due to the lateral load; that is,

$$y_o = \frac{\frac{1}{2} \rho D_o C_{L_o} v_w^2}{k} \quad (C7)$$

which yields the amplitude magnification factor in the form

$$\frac{\bar{y}}{y_o} = \frac{1}{\left\{ \left[1 - \left(\frac{\omega_k}{\omega_n} \right)^2 \right]^2 + \left(2\zeta \frac{\omega_k}{\omega_n} \right)^2 \right\}^{1/2}} \quad (C8)$$

By using equation (C6), the amplitude can be determined for a given static loading on the cylinder as a function of wind speed v_w where ω_k is replaced by $N_{Str} v_w / D_o$. (See eq. (17).)

Equation (C6) was used to predict the air-vessel steady-state response given in figure 14. The static solutions for given wind loadings were obtained from a finite-element model formulated for the SNAP (Structural Network Analyses

APPENDIX C

Program). (See refs. 16 and 17.) The adequacy of the finite-element model was verified by field measurements of the natural frequency of the air vessel. With this approach, the amplitudes of motion and associated stresses at resonance were used as a basis for evaluating structural integrity under the influence of winds.

REFERENCES

1. Hudson, C. Michael; Newman, J. C., Jr.; and Lewis, Peter E.: An Investigation of Fracture Toughness, Fatigue-Crack Growth, Sustained-Load Flow Growth, and Impact Properties of Three Pressure Vessel Steels. NASA TM X-3316, 1975.
2. Metric Practice Guide. E 308-72, American Soc. Testing & Mater., June 1972.
3. Rules for Construction of Pressure Vessels. Division 2 - Alternative Rules. Section VIII, ASME Boiler and Pressure Vessel Code, July 1, 1974.
4. MacNeal, Richard H., ed.: The NASTRAN Theoretical Manual (Level 15). NASA SP-221(01), 1972.
5. Nondestructive Examination. Section V, ASME Boiler and Pressure Vessel Code, July 1, 1974.
6. Rules for Inservice Inspection of Nuclear Power Plant Components. Section XI, ASME Boiler and Pressure Vessel Code, July 1, 1974.
7. Paris, Paul C.: The Fracture Mechanics Approach to Fatigue. Fatigue - An Interdisciplinary Approach, John J. Burke, Norman L. Reed, and Volker Weiss, eds., Syracuse Univ. Press, 1964, pp. 107-132.
8. Forman, R. G.; Kearney, V. E.; and Engle, R. M.: Numerical Analysis of Crack Propagation in Cyclic-Loaded Structures. Trans. ASME, Ser. D, J. Basic Eng., vol. 89, no. 3, Sept. 1967, pp. 459-464.
9. Newman, J. C., Jr.: Fracture Analysis of Surface- and Through-Cracked Sheets and Plates. Eng. Fract. Mech., vol. 5, no. 3, Sept. 1973, pp. 667-689.
10. User's Manual - Martin Interactive Thermal Analysis System (Version 1.0). MDS-SPLPD-71-FD238 (REV 3). Martin Marietta Corp., Nov. 1971.
11. Bartz, D. R.: A Simple Equation for Rapid Estimation of Rocket Nozzle Convective Heat Transfer Coefficients. Jet Propulsion (Tech. Notes), vol. 27, no. 1, Jan. 1957, pp. 49-51.
12. Chen, Y. N.: Flow-Induced Vibration and Noise in Tube-Bank Heat Exchangers Due to Von Karman Streets. Trans. ASME, Ser. B: J. Eng. Ind., vol. 90, no. 1, Feb. 1968, pp. 134-146.
13. Jones, George W., Jr.; Cincotta, Joseph H.; and Walker, Robert W.: Aerodynamic Forces on a Stationary and Oscillating Circular Cylinder at High Reynolds Numbers. NASA TR R-300, 1969.
14. Steel Pipe Flanges and Flanged Fittings. USAS B16.5 - 1968. American Soc. Mech. Eng., c.1968.

15. Leckie, F. A.; and Penny, R. K.: Stress Concentration Factors for the Stresses at Nozzle Intersections in Pressure Vessels. Bull. No. 90, Welding Res. Counc., Sept. 1963, pp. 19-26.
16. Whetstone, W. D.: Structural Network Analysis Program - User's Manual. Static Analysis Version V70E. LMSC-HREC D162812. Lockheed Missiles & Space Co., Dec. 14, 1970.
17. Whetstone, W. D.: Computer Analysis of Large Linear Frames. J. Struct. Div., American Soc. Civil Eng., vol. 95, no. ST11, Nov. 1969, pp. 2401-2417.

TABLE I.- DIMENSIONS AND CHARACTERISTICS OF AIR STORAGE VESSELS

[See fig. 2]

Vessel parameter	Dimension or characteristic	Remarks
Overall length, m (ft)	18.72 (61.417)	Pressure-vessel steel developed by A. O. Smith
Inside diameter, m (in.)	1.52 (60)	
Large-nozzle inside diameter, mm (in.)	165.1 ($6\frac{1}{2}$)	
Large-nozzle material	VMS 5002	
Inside-corner radius on large nozzle, mm (in.)	50.8 (2)	
Outside-corner radius on large nozzle, mm (in.)	38.1 ($1\frac{1}{2}$)	
Small-nozzle inside diameter, mm (in.)	50.8 (2)	
Small-nozzle material	VMS 5002	
Inside-corner radius on small nozzle, mm (in.)	6.4 (1/4)	
Outside-corner radius on small nozzle, mm (in.)	12.7 (1/2)	
Head configuration	Hemispherical	Innermost wall thickness, 25.4 mm (1 in.); remain- ing 17 wall thicknesses, 6.4 mm (1/4 in.) Pressure-vessel steel developed by A. O. Smith
Head thickness, mm (in.)	111.1 ($4\frac{3}{8}$)	
Head material	ASTM A-225 Gr.B	
Wall thickness, mm (in.)	138.1 ($5\frac{7}{16}$)	
Wall construction	Multilayer	
Wall material	VMS 1146A	
Design pressure, MPa (psi)	41.4 (6000)	
Capacity, m ³ (ft ³)	31.1 (1100)	
Weight, Mgm (lbm)	113.4 (250 000)	
Orientation	Vertical	

Each vessel is mounted on
a cylindrical support
skirt.

TABLE II.- DIMENSIONS AND CHARACTERISTICS OF
AIR-STORAGE-VESSEL CANISTERS

[See fig. 2]

Canister parameter	Dimension or characteristic
Length, m (ft)	16.34 (53.625)
Outside diameter, m (in.)	1.47 (58)
Head configuration	Flanged and dished
Head thickness, mm (in.)	12.7 (1/2)
Head material	ASTM A-285 Gr.C
Wall thickness, mm (in.)	9.5 (3/8)
Wall material	ASTM A-285 Gr.C

TABLE III.- DIMENSIONS AND CHARACTERISTICS OF
AIR-STORAGE-VESSEL THERMAL LINERS

[See fig. 2]

Liner parameter	Dimension or characteristic
Entrance outside diameter, mm (in.) . . .	457.2 (18)
Minimum inside diameter, mm (in.) . . .	146.1 ($5\frac{3}{4}$)
Wall thickness, mm (in.)	6.4 ($\frac{1}{4}$)
Wall material	ASTM A-283 Gr.D

TABLE IV.- DIMENSIONS AND CHARACTERISTICS OF METHANE STORAGE VESSELS

Vessel parameter	Dimension or characteristic		Remarks
	Vessel 1	Vessel 2	
Overall length, m (ft)	26.08 (85.5625)	14.12 (46.3125)	
Inside diameter, m (in.)	1.52 (60)	1.52 (60)	
Large-nozzle inside diameter, mm (in.)	81.3 (3.2)	81.3 (3.2)	
Large-nozzle material	VMS 5002	VMS 5002	Pressure-vessel steel developed by A. O. Smith
Inside-corner radius on large nozzle, mm (in.)	6.4 (1/4)	6.4 (1/4)	
Outside-corner radius on large nozzle, mm (in.)	12.7 (1/2)	12.7 (1/2)	
Small-nozzle inside diameter, mm (in.)	50.8 (2)	50.8 (2)	
Small-nozzle material	VMS 5002	VMS 5002	Pressure-vessel steel developed by A. O. Smith
Inside-corner radius on small nozzle, mm (in.)	6.4 (1/4)	6.4 (1/4)	
Outside-corner radius on small nozzle, mm (in.)	12.7 (1/2)	12.7 (1/2)	
Head configuration	Hemispherical	Hemispherical	
Head thickness, mm (in.)	111.1 ($4\frac{3}{8}$)	111.1 ($4\frac{3}{8}$)	
Head material	ASTM A-225 Gr.B	ASTM A-225 Gr.B	
Wall thickness, mm (in.)	133.4 ($5\frac{1}{4}$)	133.4 ($5\frac{1}{4}$)	
Wall construction	Multilayer	Multilayer	Innermost wall thickness, 12.7 mm (1/2 in.); remain- ing 17 wall thicknesses, 6.4 mm (1/4 in.)
Wall material	VMS 1146A	VMS 1146A	
Design pressure, MPa (psi)	41.4 (6000)	41.4 (6000)	Pressure-vessel steel developed by A. O. Smith
Capacity, m ³ (ft ³)	45.4 (1605)	23.6 (835)	
Weight, Mgm (lbm)	145.1 (320 000)	77.1 (170 000)	
Orientation	Horizontal	Horizontal	Both vessels are mounted on saddle supports.

TABLE V.- TEMPERATURES AT WHICH STEELS WERE JUDGED
TO MEET CODE-BASED IMPACT REQUIREMENTS

(a) Charpy impact tests

Steel	Temperature	
	K	°F
VMS 5002	255	0
VMS 1146A	255	0
A-225 Gr.B	239	-30

(b) Drop-weight impact tests

Steel	Temperature	
	K	°F
VMS 5002	255	0
VMS 1146A	<247	<-15
A-225 Gr.B	247	-15

TABLE VI.- FATIGUE LIVES CALCULATED FOR VARIOUS SECTIONS
OF THE AIR AND METHANE STORAGE VESSELS BY USING A
CODE-BASED FATIGUE ANALYSIS

Section	Predicted fatigue life, full pressure cycles
Large nozzles on air storage vessels	50 000
Large nozzles on methane storage vessels	50 000
Small nozzles on air and methane storage vessels	50 000
Head-to-wall junctures:	
Without backing strips	380 000
With backing strips	23 000
Canister-to-wall junctures . . .	1 700

TABLE VII.- DATA USED IN THE FRACTURE-MECHANICS ANALYSIS OF THE AIR AND METHANE STORAGE VESSELS

Area	Steel	a _i		c _i		t		σ_t		σ_r		$\sigma_{\max} = \sigma_t + \sigma_r$		σ_{\min}		C ₁ or C ₂		n or m	K _{Ic}	
		mm	in.	mm	in.	mm	in.	MPa	ksi	MPa	ksi	MPa	ksi	MPa	ksi	SI	U.S.		MN/m ^{3/2}	ksi-in ^{1/2}
Upper canister-to-wall junction	VMS 1146A	6.4	0.25	-----	---	25.4	1.0	190	27.5	0	0	190	27.5	0	0	---	5.8×10^{-10}	3	88	80
Large nozzle on air storage vessel	VMS 5002	9.5	0.375	127.0	5.0	127.0	5.0	303	44.0	41	6.0	344.74	90.0	0	0	---	2.11×10^{-7}	2.33	99	90
Large nozzle on methane storage vessel	VMS 5002	6.4	0.25	127.0	5.0	139.7	5.5	326	47.3	41	6.0	367.49	53.3	0	0	---	2.11×10^{-7}	2.33	99	90
Small nozzles on air and methane storage vessels . . .	VMS 5002	6.4	0.25	127.0	5.0	114.3	4.5	326	47.3	41	6.0	367.49	53.3	0	0	---	2.11×10^{-7}	2.33	99	90
Head-to-wall junction	A-225 Gr.B	12.7	0.50	127.0	5.0	111.8	4.4	181	26.3	41	6.0	222.7	32.3	0	0	---	3.75×10^{-7}	2.00	82	75

TABLE VIII.- VARIATION OF NOZZLE-AREA TEMPERATURE WITH TIME DURING A TUNNEL RUN

Time, s	Temperature for node point -																	
	1		2		3		4		5		6		7		8		9	
	K	°F	K	°F	K	°F	K	°F	K	°F	K	°F	K	°F	K	°F	K	°F
0	266.5	20.00	266.5	20.00	266.5	20.00	266.5	20.00	266.5	20.00	266.5	20.00	266.5	20.00	266.5	20.00	266.5	20.00
20	266.3	19.69	266.3	19.91	266.4	19.89	266.4	19.84	266.2	19.54	266.1	19.36	265.7	18.61	266.5	19.99	266.5	19.99
40	265.8	18.82	266.3	19.66	266.2	19.56	266.1	19.38	265.6	18.33	265.2	17.73	264.2	15.83	266.5	19.95	266.5	19.94
60	265.1	17.46	266.1	19.23	265.9	19.01	265.7	18.63	264.6	16.53	263.9	15.43	262.3	12.52	266.4	19.85	266.4	19.83
80	264.1	15.66	265.7	18.62	265.5	18.24	265.2	17.60	263.3	14.27	262.4	12.64	260.3	8.91	266.3	19.66	266.3	19.62
100	262.8	13.46	265.3	17.83	265.0	17.26	264.4	16.30	261.8	11.62	260.6	9.46	258.2	5.03	266.1	19.38	266.1	19.32
120	261.4	10.88	264.7	16.86	264.3	16.06	263.6	14.72	260.2	8.63	258.7	5.95	255.9	.90	265.9	19.00	265.9	18.92
140	259.8	7.95	264.1	15.70	263.5	14.64	262.5	12.87	258.3	5.31	256.6	2.14	253.4	-3.52	265.6	18.49	265.6	18.39
160	257.9	4.65	263.3	14.34	262.6	12.99	261.3	10.74	256.3	1.67	254.3	-2.00	250.8	-8.28	265.3	17.86	265.2	17.76
180	255.9	1.00	262.5	12.77	261.5	11.10	260.0	8.33	254.1	-2.30	251.8	-6.49	247.9	-13.41	264.9	17.09	264.8	16.99
200	253.7	-3.04	261.5	10.98	260.3	8.95	258.5	5.61	251.7	-6.64	249.1	-11.36	244.8	-19.00	264.4	16.17	264.3	16.09

Time, s	Temperature for node point -																	
	10		11		12		13		14		15		16		17		18	
	K	°F	K	°F	K	°F	K	°F	K	°F	K	°F	K	°F	K	°F	K	°F
0	266.5	20.00	266.5	20.00	266.5	20.00	266.5	20.00	266.5	20.00	266.5	20.00	266.5	20.00	266.5	20.00	266.5	20.00
20	266.5	19.97	266.0	19.13	266.5	19.97	266.5	19.98	266.5	19.96	266.5	20.00	266.5	20.00	266.5	20.00	266.5	19.99
40	266.4	19.82	265.2	17.65	266.4	19.87	266.4	19.93	266.4	19.82	266.4	19.97	266.5	20.00	266.5	19.99	266.4	19.94
60	266.2	19.54	264.2	15.93	266.3	19.68	266.4	19.83	266.3	19.61	266.4	19.88	266.5	19.98	266.5	19.97	266.4	19.83
80	266.0	19.12	263.2	14.02	266.2	19.42	266.3	19.70	266.1	19.32	266.3	19.71	266.5	19.95	266.4	19.93	266.3	19.62
100	265.7	18.56	262.0	11.94	266.0	19.07	266.2	19.52	265.9	18.96	266.2	19.46	266.4	19.90	266.4	19.87	266.1	19.32
120	265.3	17.88	260.7	9.67	265.7	18.62	266.1	19.30	265.7	18.53	266.0	19.11	266.4	19.82	266.4	19.78	265.9	18.92
140	264.8	17.06	259.4	7.21	265.4	18.09	265.9	19.03	265.4	18.03	265.7	18.65	266.3	19.71	266.3	19.67	265.6	18.40
160	264.3	16.10	257.9	4.52	265.1	17.46	265.8	18.70	265.1	17.46	265.4	18.09	266.2	19.55	266.2	19.53	265.3	17.76
180	263.7	14.99	256.3	1.59	264.7	16.72	265.5	18.32	264.7	16.82	265.0	17.41	266.1	19.35	266.1	19.36	264.8	16.99
200	263.0	13.74	254.5	-1.63	264.2	15.88	265.3	17.88	264.3	16.10	264.6	16.62	266.0	19.09	266.0	19.15	264.3	16.10

TABLE VIII.- Concluded

Time, s	Temperature for node point -																	
	19		20		21		22		23		24		25		26		27	
	K	°F	K	°F	K	°F	K	°F	K	°F	K	°F	K	°F	K	°F	K	°F
0	266.5	20.00	266.5	20.00	266.5	20.00	266.5	20.00	266.5	20.00	266.5	20.00	266.5	20.00	266.5	20.00	266.5	20.00
20	266.5	20.00	266.5	20.00	266.5	20.00	264.7	16.69	264.7	16.85	264.6	16.69	264.6	16.70	264.8	16.89	264.6	16.70
40	266.5	20.00	266.5	20.00	266.5	20.00	262.6	13.09	262.8	13.36	262.6	13.09	262.6	13.10	262.9	13.47	262.6	13.10
60	266.5	19.98	266.5	20.00	266.5	20.00	260.5	9.29	260.7	9.67	260.5	9.30	260.5	9.30	260.9	9.87	260.5	9.31
80	266.5	19.95	266.5	20.00	266.5	20.00	258.3	5.28	258.6	5.76	258.3	5.29	258.3	5.29	258.7	6.05	258.3	5.29
100	266.4	19.90	266.5	20.00	266.5	20.00	255.9	1.01	256.3	1.61	255.9	1.03	255.9	1.04	256.5	1.99	255.9	1.04
120	266.4	19.81	266.5	20.00	266.5	20.00	253.4	-3.53	253.8	-2.81	253.4	-3.51	253.4	-3.50	254.1	-2.33	253.4	-3.50
140	266.3	19.69	266.5	19.99	266.5	19.99	250.7	-8.40	251.2	-7.56	250.7	-8.38	250.7	-8.36	251.5	-6.97	250.7	-8.36
160	266.2	19.53	266.5	19.99	266.5	19.99	247.8	-13.65	248.3	-12.67	247.8	-13.62	247.8	-13.61	248.7	-11.97	247.8	-13.61
180	266.1	19.32	266.5	19.98	266.5	19.98	244.6	-19.35	245.2	-18.23	244.6	-19.32	244.6	-19.30	245.7	-17.40	244.6	-19.30
200	266.0	19.06	266.5	19.97	266.5	19.97	241.2	-25.59	241.9	-24.32	241.2	-25.55	241.2	-25.53	242.4	-23.35	241.2	-25.53

TABLE IX.- INSPECTION PLAN FOR THE AIR AND METHANE STORAGE VESSELS AT THE LANGLEY 8-FOOT HIGH-TEMPERATURE STRUCTURES TUNNEL

Designation	Component	Drawing no.	Item index no.	Inspection schedule						Inspection requirements
				1975 or N _F = 40	1976 or N _F = 80	1977 or N _F = 120	1978 or N _F = 160	1980 or N _F = 240	1985 or N _F = 440	
I.A.	Large nozzles									
I.A.1	(1) All	LE-704302	23					UT-shear	UT-shear	A qualified inspector shall inspect the inside-corner radius of the large nozzles on each air and methane storage vessel. The inspector shall use the existing shoes and 12.7-mm by 25.4-mm (1/2-in. by 1-in.) 2.25-MHz transducer combination developed for the initial inspections of these nozzles. The inspector shall calibrate his equipment by using the existing calibration standard.
I.A.2	(2) Large nozzle producing linear indication after modification	LE-704302	23					PT	PT	A qualified inspector shall inspect the inside nozzle area of the large nozzle producing a linear UT indication. The inspector shall use the procedures outlined in Section V of the 1974 ASME B & PV Code in making this inspection.
I.B.	Small nozzles									
I.B.1	(1) All	LE-704302	22					UT-shear	UT-shear	A qualified inspector shall inspect the inside-corner radius of the small nozzles on each air and methane storage vessel. The inspector shall use the existing shoes and 12.7-mm by 25.4-mm (1/2-in. by 1-in.) 2.25-MHz transducer combination developed for the initial inspection of these nozzles. The inspector shall calibrate his equipment by using the existing calibration standard.
I.B.2	(2) Two small nozzles producing linear indications	LE-704302	22	PT	PT	PT	PT	PT	PT	A qualified inspector shall inspect the inside nozzle area of the two nozzles producing linear UT indications. The inspector shall use the procedures outlined in Section V of the 1974 ASME B & PV Code in making this inspection.

TABLE IX.- Concluded

Designation	Component	Drawing no.	Item index no.	Inspection schedule						Inspection requirements
				1975 or N _F = 40	1976 or N _F = 80	1977 or N _F = 120	1978 or N _F = 160	1980 or N _F = 240	1985 or N _F = 440	
I.C.	Head-to-wall juncture	LE-704302	C-1 and C-7							UT-shear A qualified inspector shall inspect the welds joining the hemispherical heads to the cylindrical walls of the air and methane storage vessels. The inspector shall use a 12.7-mm by 25.4-mm (1/2-in. by 1-in.) 2.25-MHz transducer in making this inspection. The inspector shall calibrate his equipment by using the existing calibration standard.
I.D.	Canister-to-wall junctures	LE-704301	48					Visual	Visual	A qualified inspector shall inspect the 1/2-in. fillet welds connecting the upper portion of the canister to the cylindrical walls of two air storage vessels. The inspector shall use the procedures outlined in Section V of the 1974 ASME B & PV Code in making this inspection. A fiber-optics borescope is available for making this inspection.
I.E.	Hemispherical heads									
I.E.1	(1) Three vessels indicating complete loss of back reflection	LE-704302	101	UT-long	UT-long			UT-long	UT-long	A qualified inspector shall inspect the hemispherical heads of the three vessels indicating complete loss of back reflection. The inspector shall use the procedures outlined in Section V of the 1974 ASME B & PV Code in making this inspection. The inspector shall trace in paint, as closely as practicable, the circumferences of all laminations located during this inspection.
I.E.2	(2) All other heads									No inspection required unless inspectors find lamination growth in I.E.1.

TABLE X.- COMPARISON OF THE TENSILE AND CHEMICAL PROPERTIES OF THE NEW STEELS
TESTED WITH THE STEELS IN THE STORAGE VESSELS

(a) Tensile properties

Steel	Status	σ_u		$\sigma_{u,min}$		σ_y		$\sigma_{y,min}$		e, percent
		MPa	ksi	MPa	ksi	MPa	ksi	MPa	ksi	
VMS 5002	In vessel Tested	673	97.6	641	93	466	67.6	448	65	23
		675	97.9			507	73.5			28
VMS 1146A	In vessel Tested	772	112.0	724	105	585	84.9	483	70	32
		698	101.3			517	75.0			31
A-225 Gr.B	In vessel Tested	538	78.1	517	75	378	54.8	296	43	30
		566	82.1			403	58.4			34

(b) Chemical properties

Steel	Status	Percent of element -						
		C	Mn	P	S	Si	V	Ni
VMS 1146A	In vessel Tested	0.22	1.30	0.015	0.027	0.28	0.15	0.57
		.21	1.31	.014	.024	.28	.15	.55
VMS 5002	In vessel Tested	0.24	1.52	0.017	0.022	0.26	0.15	0.59
		.23	1.45	.015	.023	.30	.15	.59
A-225 Gr.B	In vessel Tested	0.17	1.30	0.012	0.024	0.22	0.11	----
		.15	1.27	.013	.026	.27	.12	----

TABLE XI.- CALCULATED S_m VALUES FOR VMS 5002, VMS 1146A,
AND ASTM A-225 Gr.B STEELS

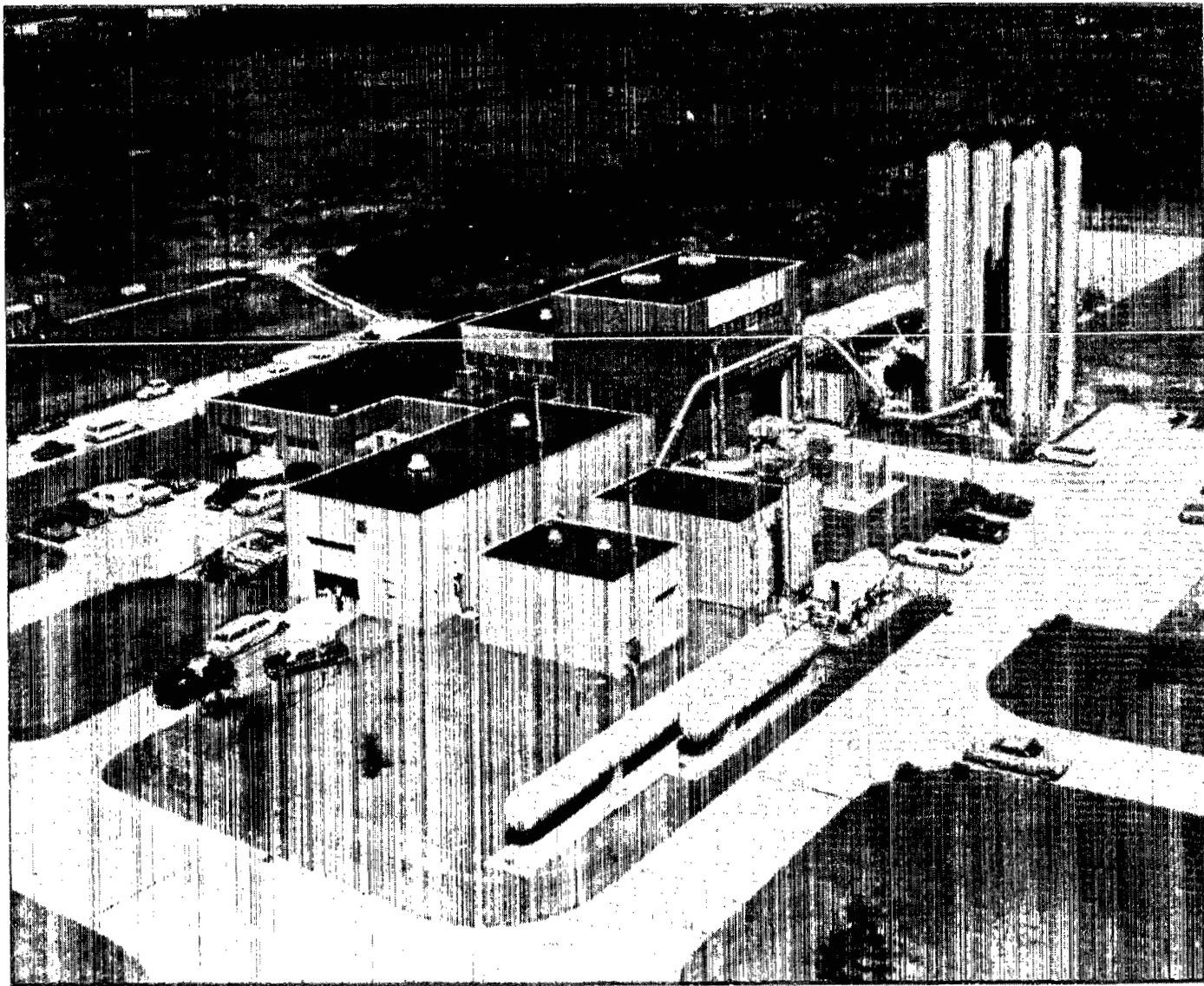
Steel	Location	S_m	
		MPa	ksi
VMS 5002	Nozzles	214	31
VMS 1146A	Cylindrical walls	241	35
A-225 Gr.B	Spherical walls	172	25

TABLE XII.- MAXIMUM ALLOWABLE VALUES OF STRESS INTENSITIES FOR THE THREE PRESSURE-VESSEL STEELS

$S_{p,m,max} = S_m$ (see Code paragraph 4-131)						$S_{l,m,max} = 1.5S_m$ (see Code paragraph 4-132)						$S_{p,s,max} = 3S_m$ (see Code paragraph 4-134)					
VMS 5002		VMS 1146A		A-225 Gr.B		VMS 5002		VMS 1146A		A-225 Gr.B		VMS 5002		VMS 1146A		A-225 Gr.B	
MPa	ksi	MPa	ksi	MPa	ksi	MPa	ksi	MPa	ksi	MPa	ksi	MPa	ksi	MPa	ksi	MPa	ksi
214	31	241	35.0	172	25.0	321	46.5	362	52.5	259	37.5	641	93	724	105	517	75.0

TABLE XIII.- HEAD AND WALL STRESSES AT THE HEAD-TO-WALL JUNCTURE

Stressed area	$\sigma_{t,o}$		$\sigma_{t,in}$		$\sigma_{l,o}$		$\sigma_{l,in}$		$\sigma_{r,o}$		$\sigma_{r,in}$	
	MPa	ksi	MPa	ksi	MPa	ksi	MPa	ksi	MPa	ksi	MPa	ksi
Wall Head	152	22.1	210	30.5	77	11.1	132	19.2	0	0	-41	-6
	183.4	26.6	201	29.2	155.1	22.5	90	13.1	0	0	-41	-6



L-69-6791

Figure 1.- Aerial view of the Langley 8-foot high-temperature structures tunnel.

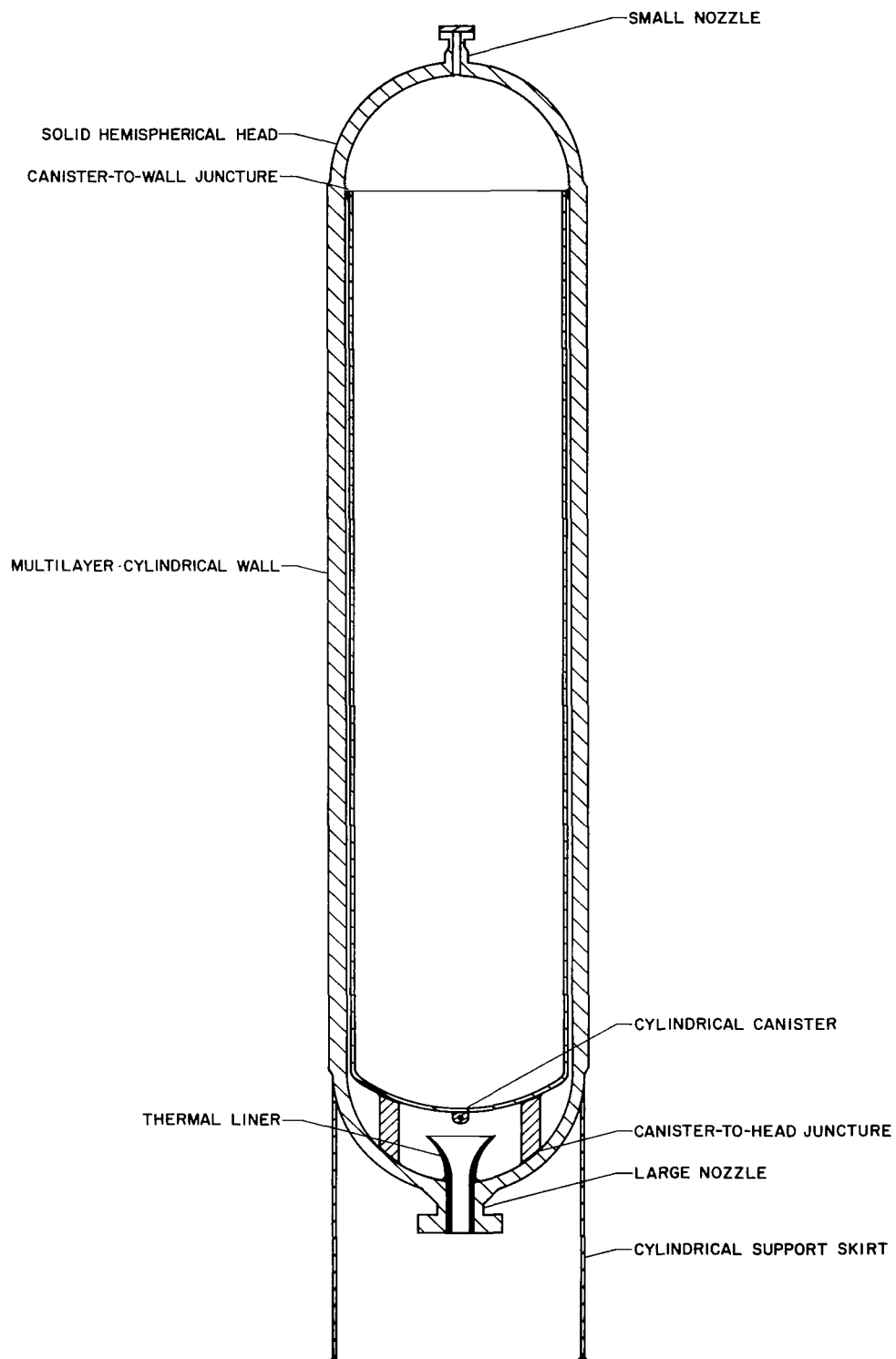


Figure 2.- Cross-sectional view of a typical air storage vessel at the Langley 8-foot high-temperature structures tunnel.

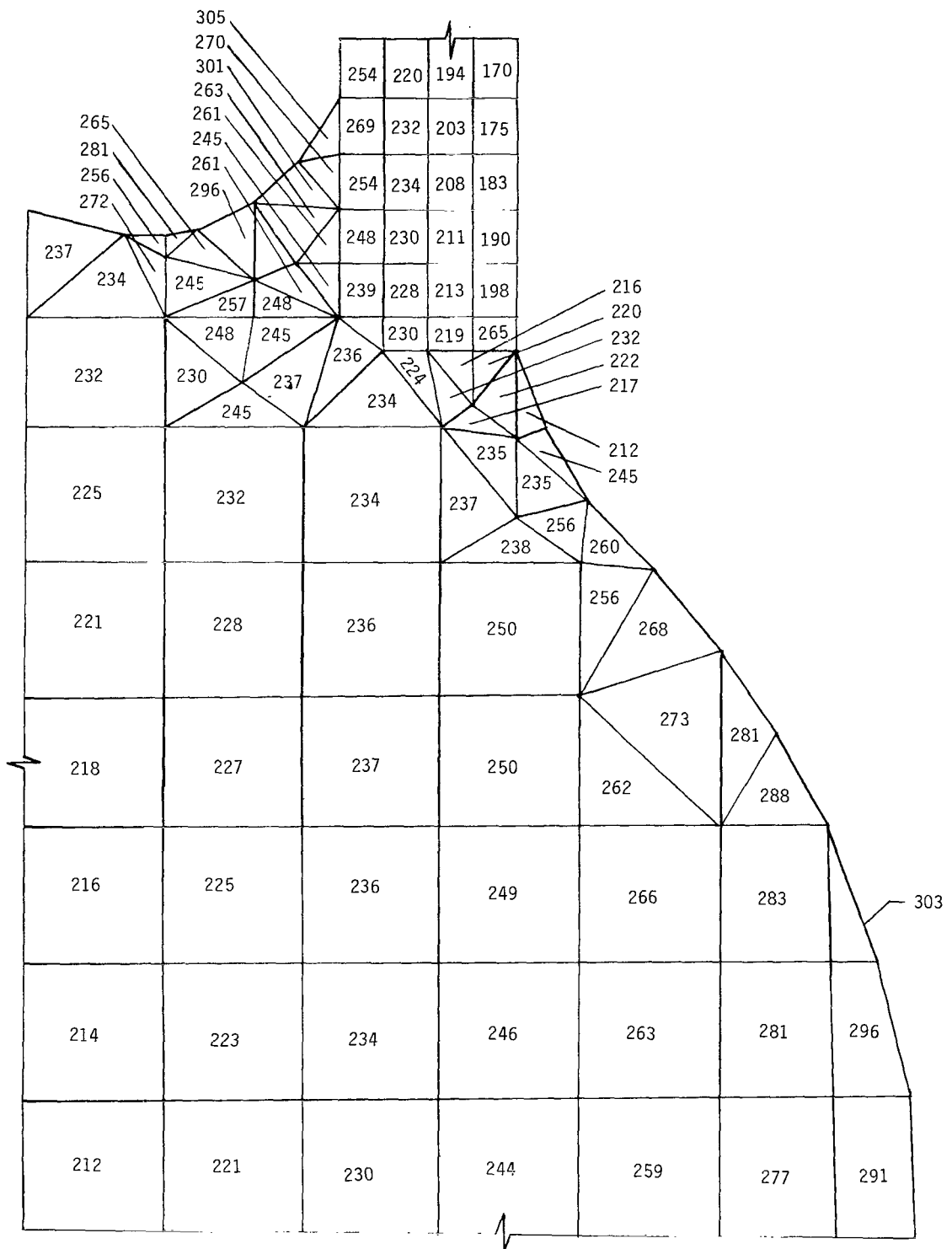
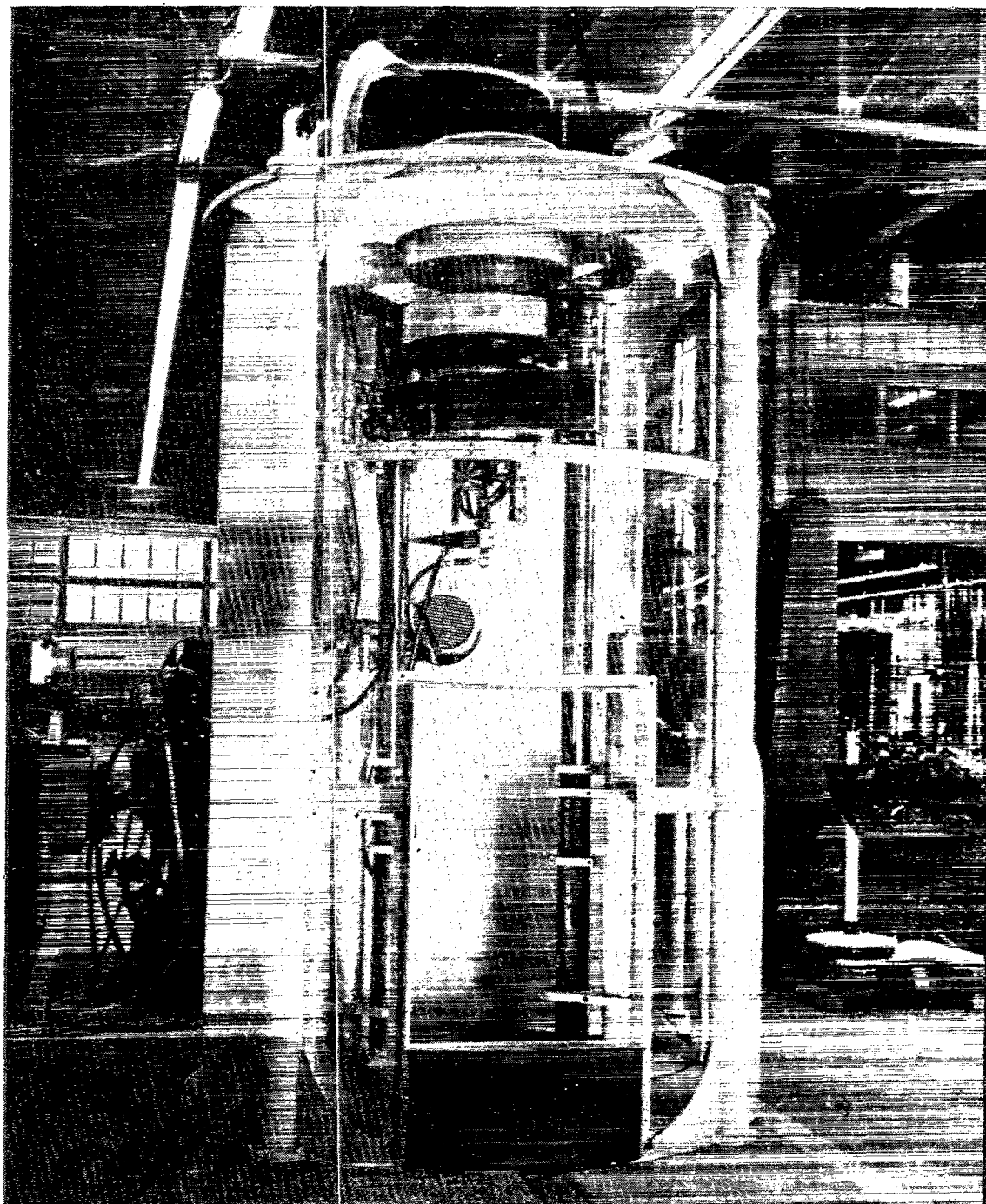


Figure 3.- Tangential stresses in nozzle area of air storage vessel.
Stresses (given in MPa) were computed prior to nozzle modification.



L-73-7776

Figure 4.- Nozzle mock-up and contour-grinding machine used to modify the air-vessel nozzles.

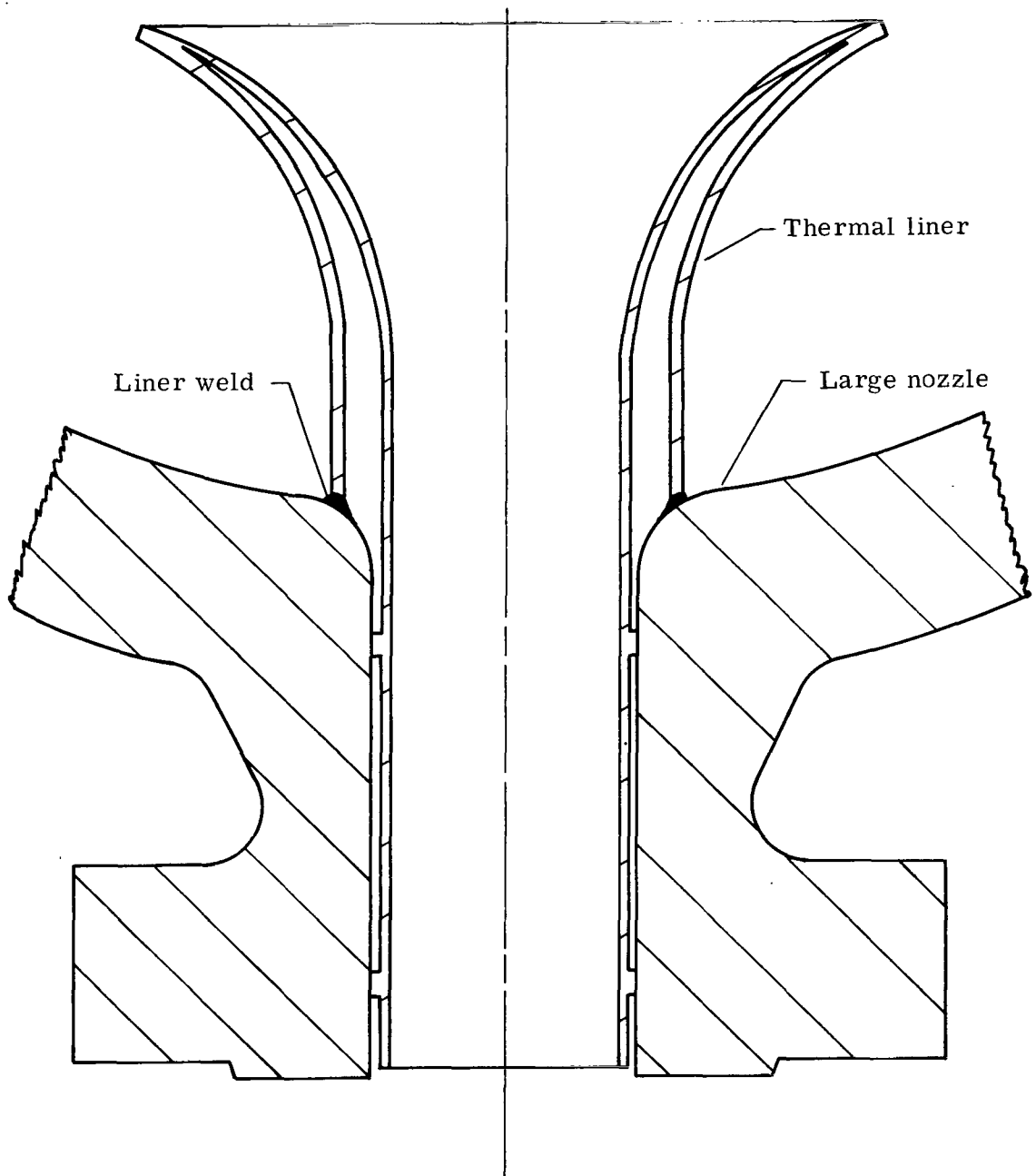


Figure 5.- Cross-sectional view of air-storage-vessel nozzles prior to modification.

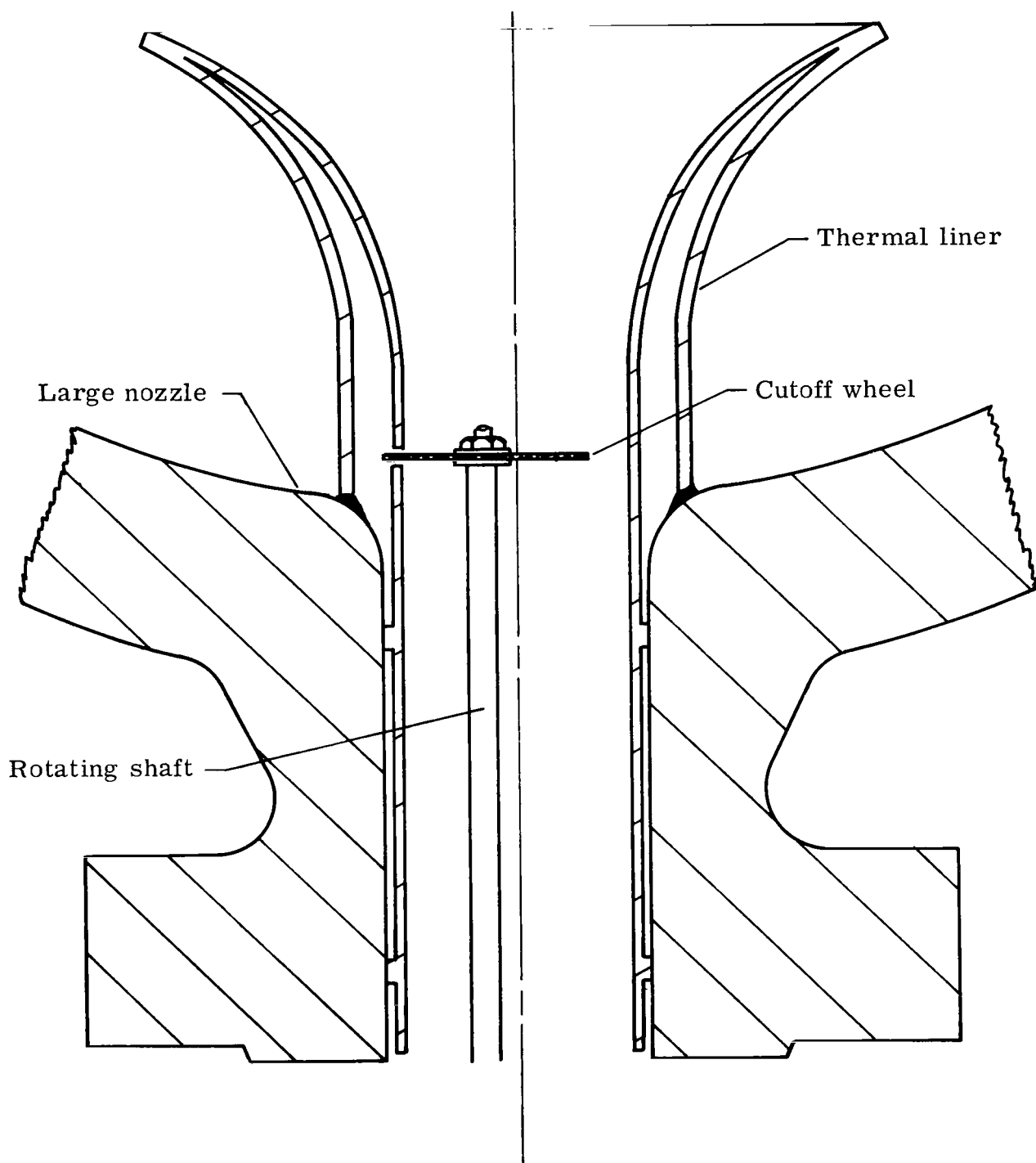


Figure 6.- Cross-sectional view of air-storage-vessel nozzles with inside section of liner being removed.

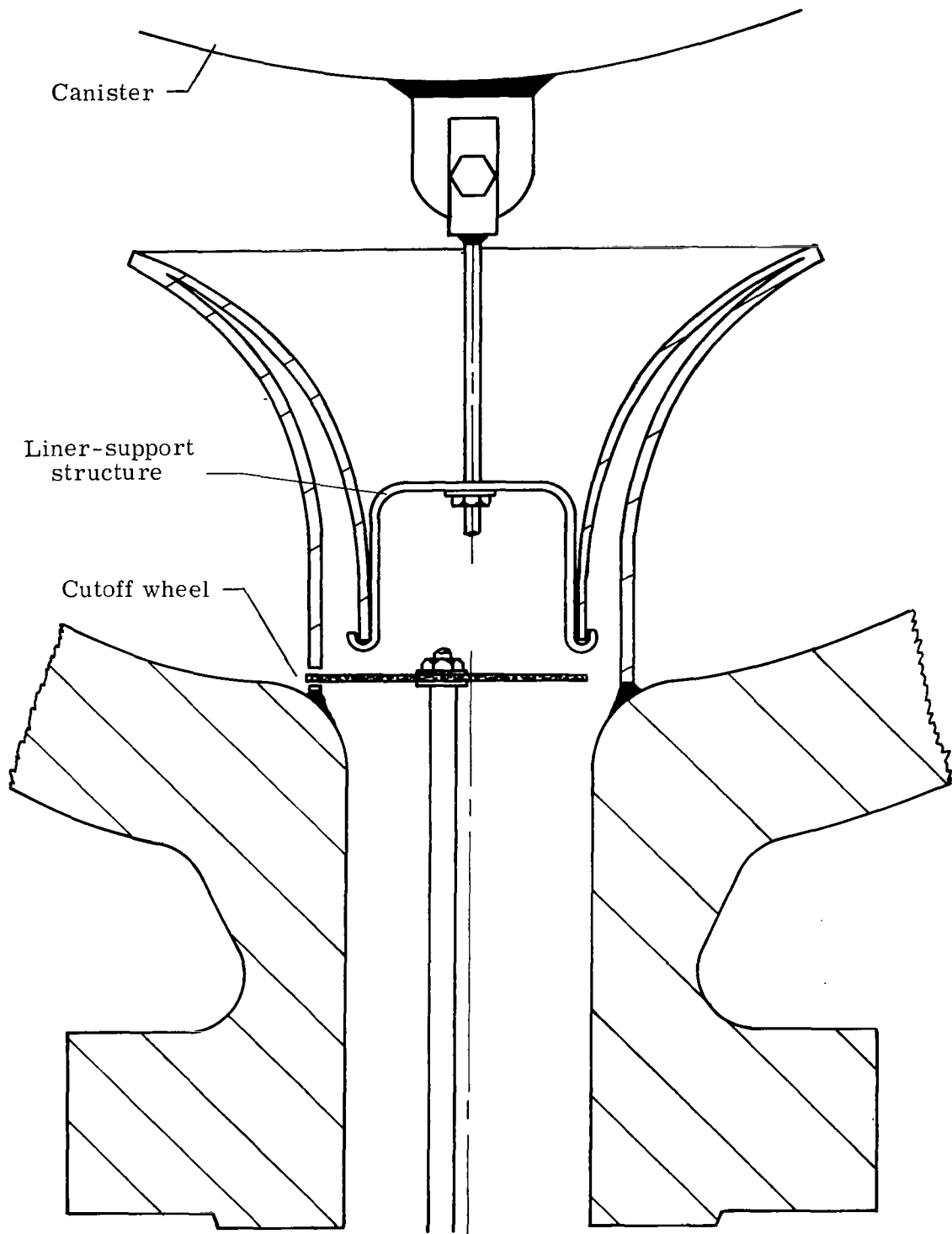


Figure 7.- Cross-sectional view of air-storage-vessel nozzles with outside section of liner being removed.

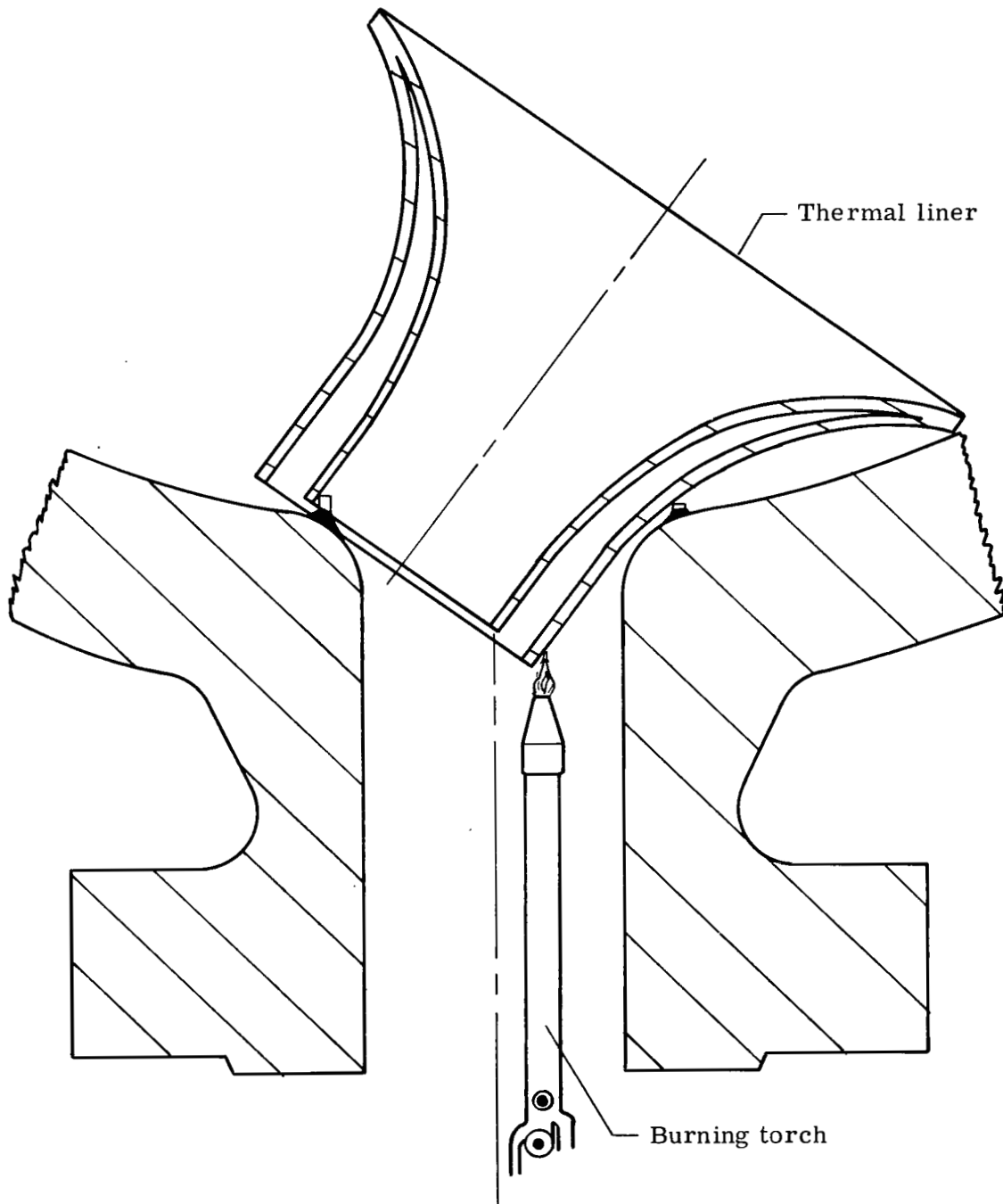


Figure 8.- Cross-sectional view of air-storage-vessel nozzles depicting liner fragmentation.

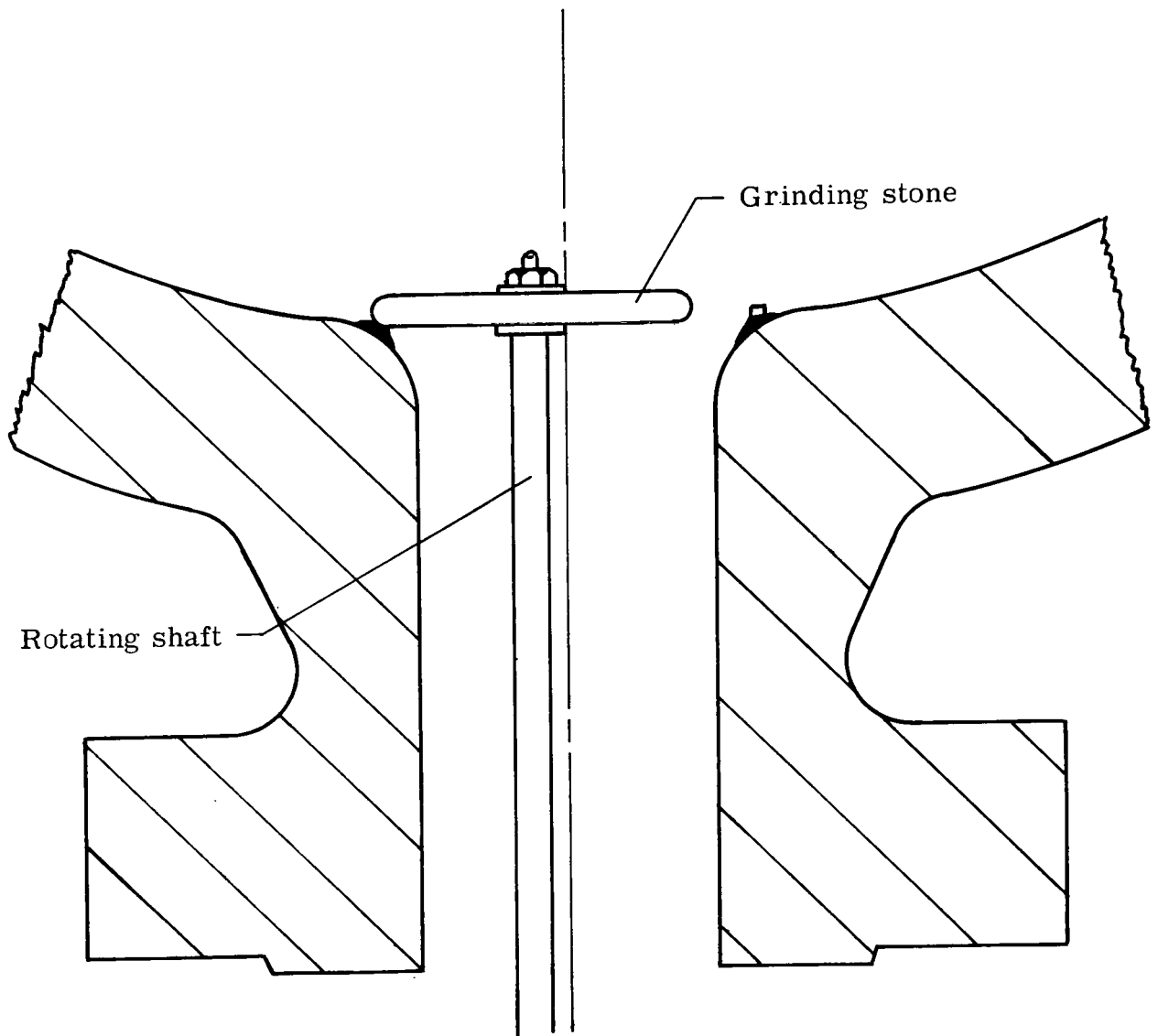


Figure 9.- Cross-sectional view of air-storage-vessel nozzles with inside-corner radius being recontoured.

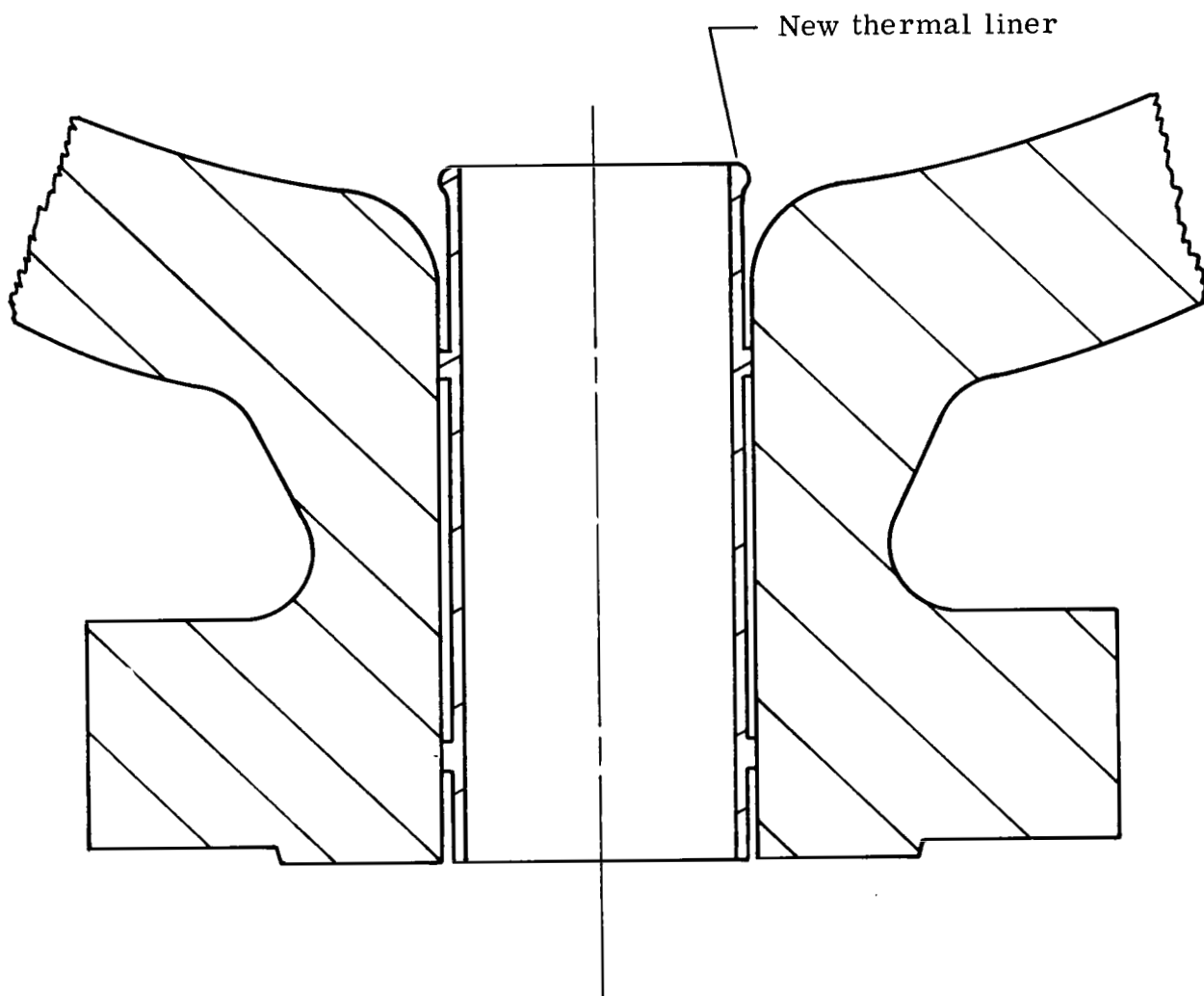


Figure 10.- Cross-sectional view of modified air-storage-vessel nozzles.

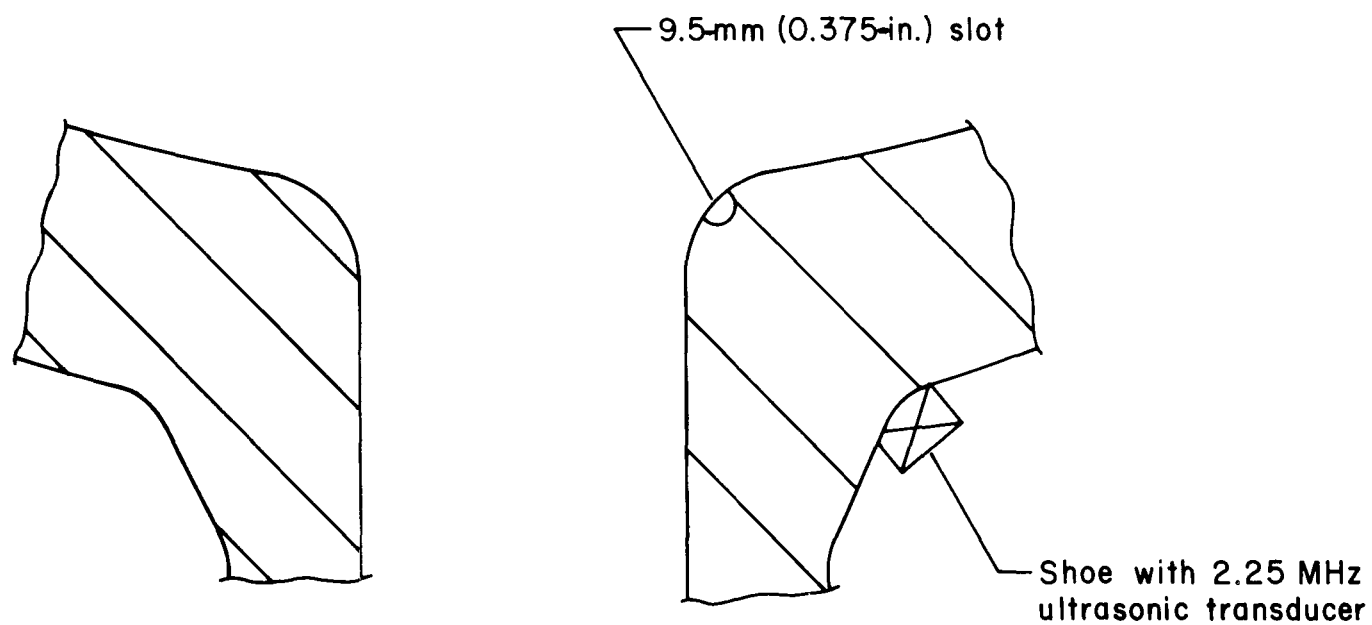


Figure 11.- Cross-sectional view of large-nozzle mock-up for air storage vessels.

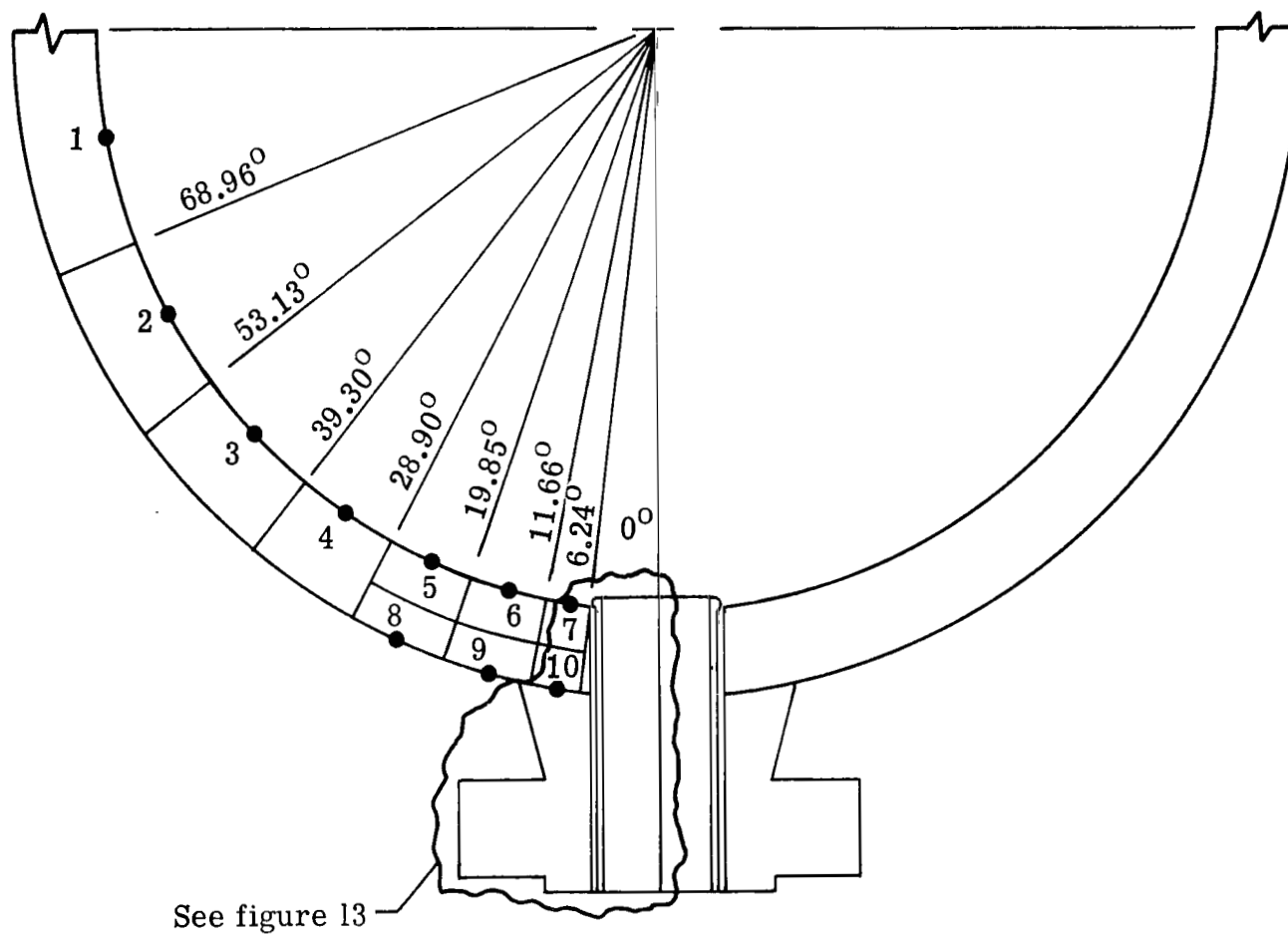


Figure 12.- Node points 1 to 10 near the large nozzle at which temperatures were calculated for an extreme tunnel run. Table VIII presents the calculated temperatures.

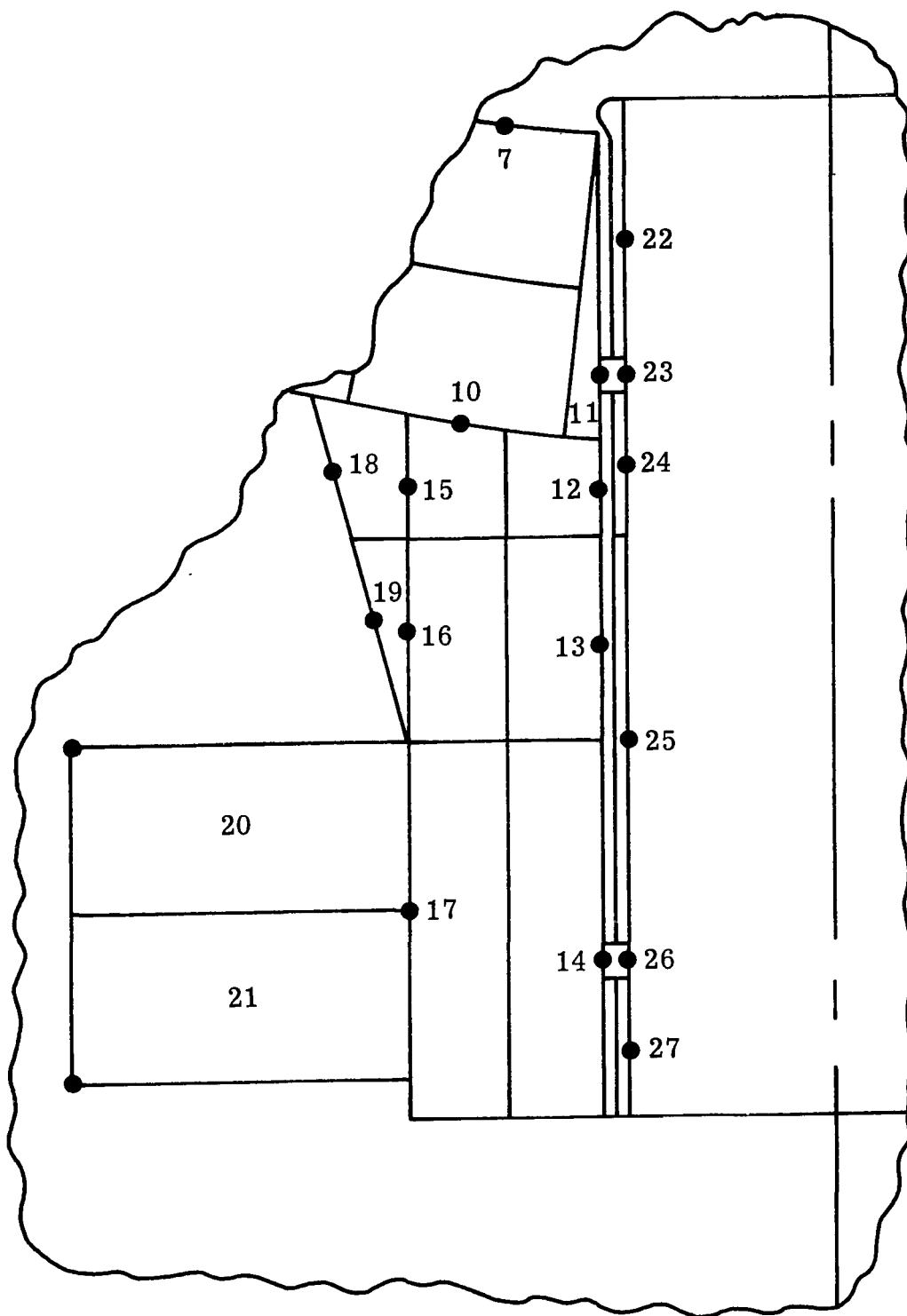


Figure 13.- Node points 7 and 10 to 27 near the large nozzle at which temperatures were calculated for an extreme tunnel run. Table VIII presents the calculated temperatures.

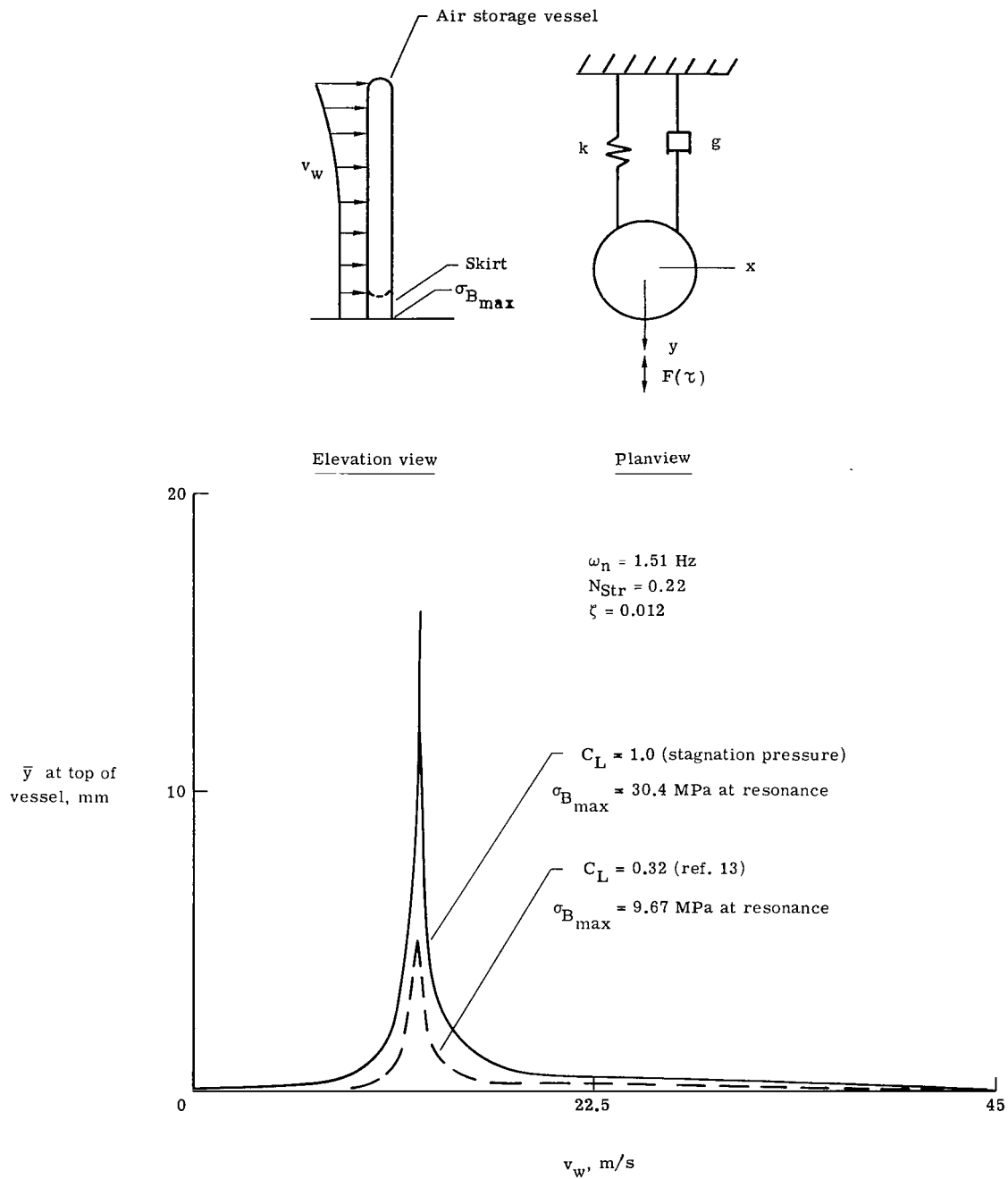


Figure 14.- Mathematical model and predicted response characteristics of an air storage vessel.

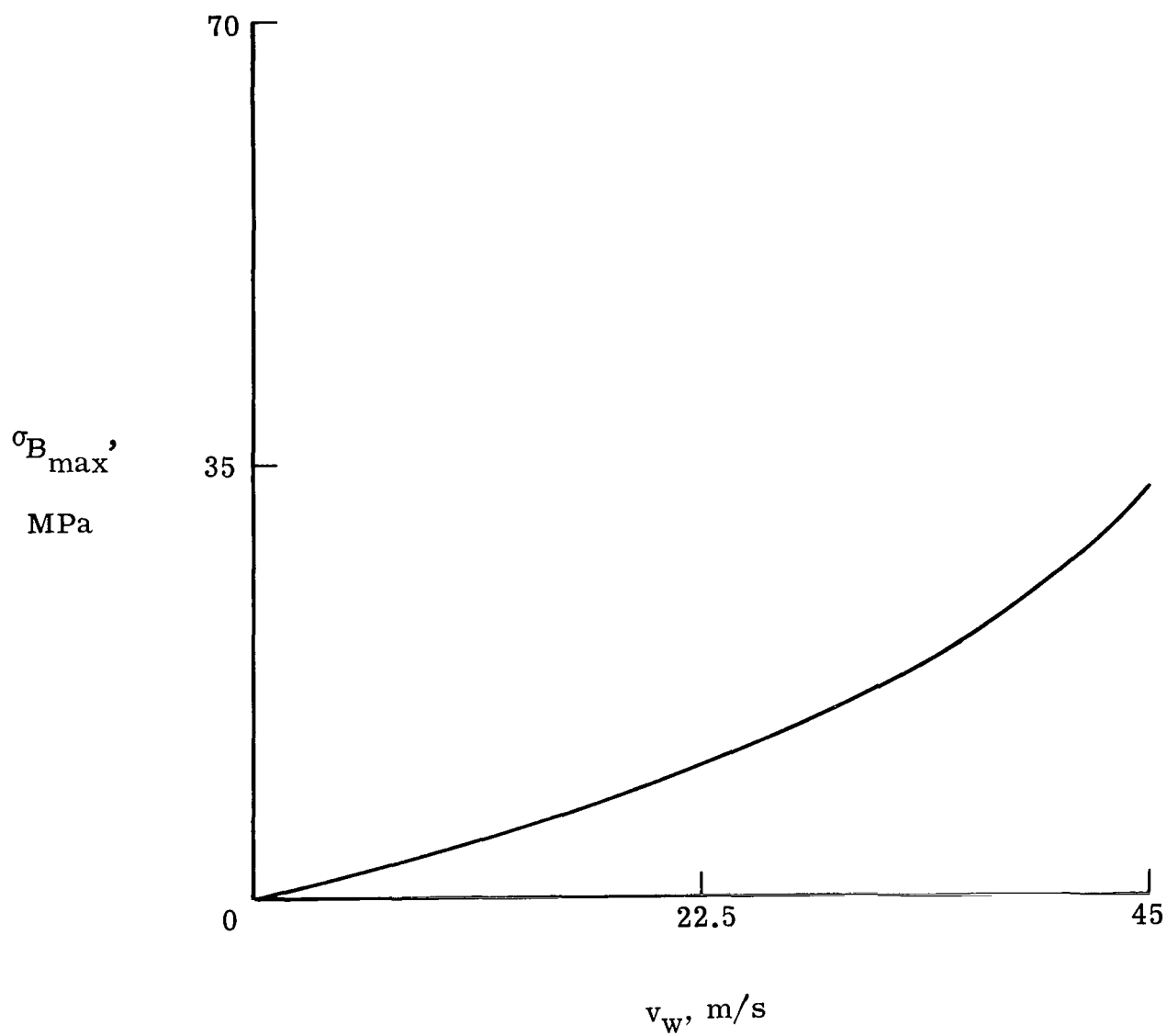
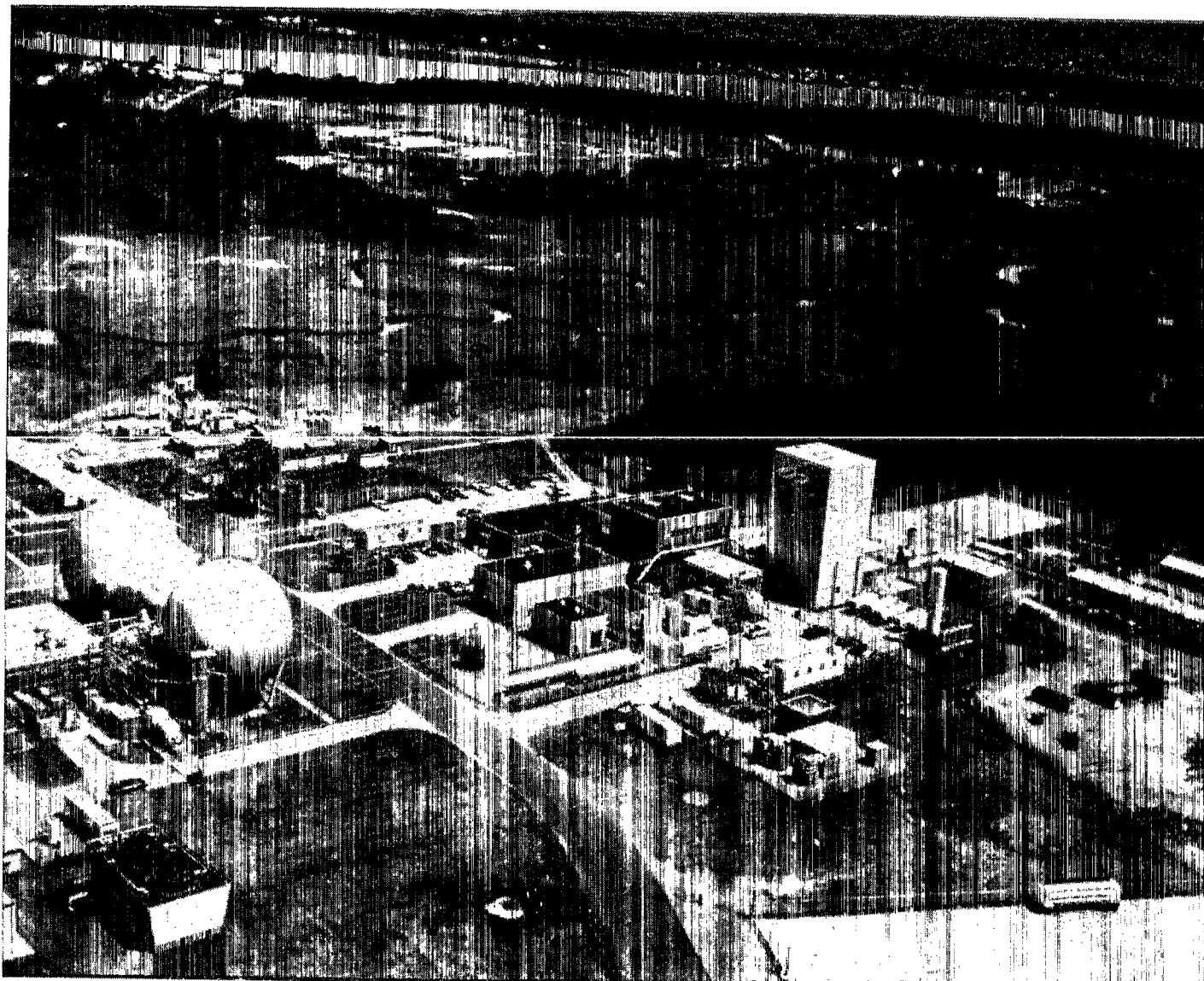


Figure 15.- Variation of stress at the base of an air storage vessel with steady wind velocity. $C_D = 1.0$.



L-76-5263

Figure 16.- Aerial view of the Langley 8-foot high-temperature structures tunnel including the thermal enclosure over the air storage vessels.

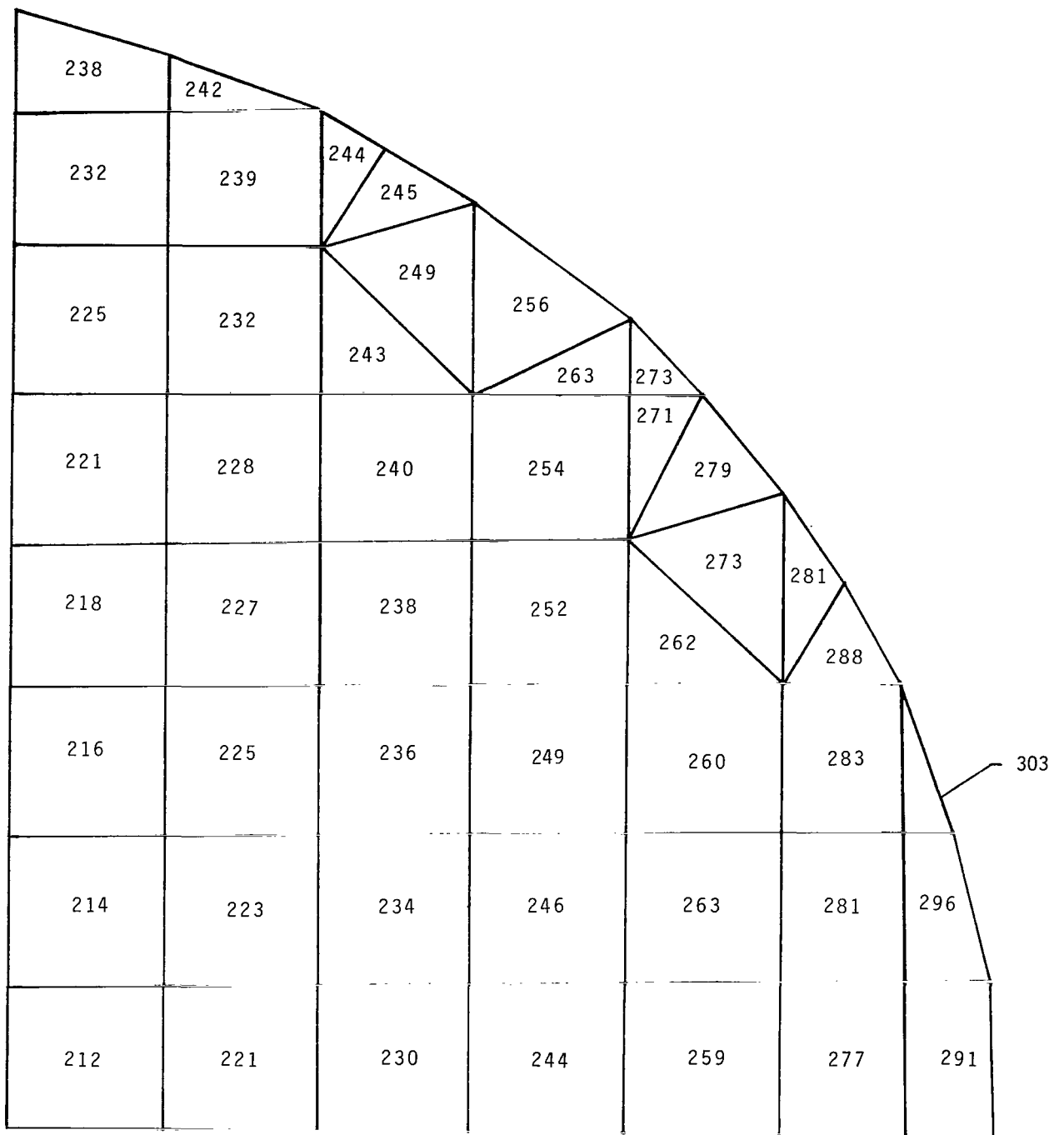


Figure 17.- Tangential stress in modified nozzle area of air storage vessels.
Stresses are given in MPa.

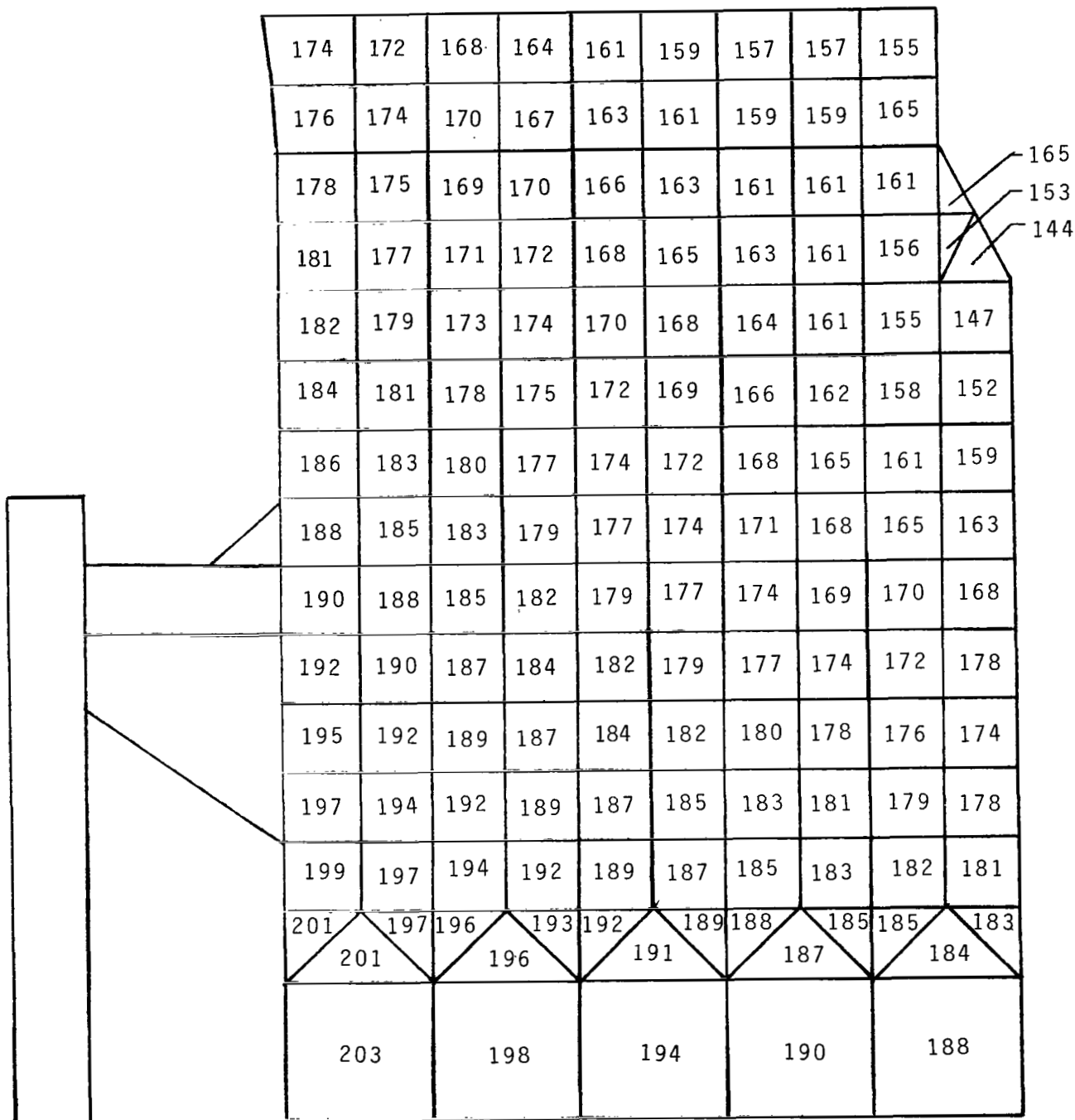


Figure 18.- Tangential stresses for upper head-to-wall juncture area of air storage vessels. Stresses are given in MPa.



077 001 C1 U D 770128 S00903DS
DEPT OF THE AIR FORCE
AF WEAPONS LABORATORY
ATTN: TECHNICAL LIBRARY (SUL)
KIRTLAND AFB NM 87117

POSTMASTER: If Undeliverable (Section 158
Postal Manual) Do Not Return

"The aeronautical and space activities of the United States shall be conducted so as to contribute . . . to the expansion of human knowledge of phenomena in the atmosphere and space. The Administration shall provide for the widest practicable and appropriate dissemination of information concerning its activities and the results thereof."

—NATIONAL AERONAUTICS AND SPACE ACT OF 1958

NASA SCIENTIFIC AND TECHNICAL PUBLICATIONS

TECHNICAL REPORTS: Scientific and technical information considered important, complete, and a lasting contribution to existing knowledge.

TECHNICAL NOTES: Information less broad in scope but nevertheless of importance as a contribution to existing knowledge.

TECHNICAL MEMORANDUMS: Information receiving limited distribution because of preliminary data, security classification, or other reasons. Also includes conference proceedings with either limited or unlimited distribution.

CONTRACTOR REPORTS: Scientific and technical information generated under a NASA contract or grant and considered an important contribution to existing knowledge.

TECHNICAL TRANSLATIONS: Information published in a foreign language considered to merit NASA distribution in English.

SPECIAL PUBLICATIONS: Information derived from or of value to NASA activities. Publications include final reports of major projects, monographs, data compilations, handbooks, sourcebooks, and special bibliographies.

TECHNOLOGY UTILIZATION PUBLICATIONS: Information on technology used by NASA that may be of particular interest in commercial and other non-aerospace applications. Publications include Tech Briefs, Technology Utilization Reports and Technology Surveys.

Details on the availability of these publications may be obtained from:

SCIENTIFIC AND TECHNICAL INFORMATION OFFICE

NATIONAL AERONAUTICS AND SPACE ADMINISTRATION
Washington, D.C. 20546